CRANFIELD

CoA report No. 9312

September 1993

MULTIDIMENSIONAL WAF-TYPE SCHEMES FOR MODEL CONSERVATION LAWS

E.F.Toro and S.J.Billett

Department of Aerospace Science,
College of Aeronautics, Cranfield University,
Cranfield, Bedfordshire, MK43 OAL, ENGLAND.

Cranfield

College of Aeronautics Report No 9312
September 1993

MULTIDIMENSIONAL WAF-TYPE SCHEMES FOR MODEL CONSERVATION LAWS

E.F. Toro and S.J. Billett

College of Aeronautics
Cranfield University
Cranfield, Bedford MK43 0AL. England

ISBN 1 871564 65 4

£10.00

Abstract

We explore how the Weighted Average Flux (WAF) approach can be used to generate first and second order accurate finite volume schemes in one, two and three space dimensions. The derived schemes have multidimensional upwinding aspects and good stability properties. We construct oscillation-free methods that are second order accurate in smooth flow by making use of one-dimensional limiter functions. Some numerical results are presented.

Key words hyperbolic conservation laws, WAF-type schemes, finite volume schemes, multidimensional upwinding

1. Introduction

Upwind methods for Computational Fluid Dynamics (CFD) form a respectable class of numerical techniques available to the CFD practioner today. This is the result of an intensive research activity spanned over many years. The distinguished works of Godunov [1], van Leer [2], Roe [3], Osher [4], Harten [5], and many others, have provided a solid theoretical framework for further advancement.

An important issue is how to generalize the first order Godunov method [1] to second or higher order accuracy. Van Leer [6, 2] proposed his MUSCL approach whereby the piecewise constant cell average states are replaced by reconstructed states that admit spacial variation within each cell. A class of second-order Godunov-type methods based on this have been constructed. Examples are the PLM method of Colella [7], the GRP method of Ben-Artzi and Falcovitz [8] and the MUSCL Hancock scheme [9].

An alternative approach for constructing second-order Godunov type methods is the Weighted Average Flux (WAF) approach [10]. Its origins go back to a Random Flux approach by Toro [11] which was later proved to be second order accurate in a statistical sense (Toro and Roe [12]). The WAF approach has been shown to be successful in applications to a variety of practical problems [10], [13], [14]. Its key feature is that second order accuracy can be achieved by solving the conventional piecewise constant Riemann problem; no reconstruction/evolution steps are necessary, although such processes may also be admitted. The accuracy comes from utilising this solution averaged over space and time. This averaging takes the form of an integral of the flux, or chosen variables, over some volume.

In this paper we discuss how the WAF approach can be used to generate schemes for the solution on the linear advection equation in more than one space dimension. We generalize the approach by integrating the exact solution of multidimensional initial value problems in space and time. The initial data for these problems is the data at a given time level, which we assume constant within each cell. MUSCL type extensions are, of course, also possible, but are not explored here.

In two space dimensions we show how different integration methods can lead to numerical schemes with different accuracy and stability properties. In particular, we present two second order schemes which, as far as we know, are new. They are conservative, finite volume schemes with good stability properties, and are natural extensions of the one-dimensional Lax-Wendroff scheme [15]. Moreover, due to the nature of their derivation, they have multidimensional upwinding features. We also derive a finite volume, first order scheme that is a natural extension to Godunov's scheme [1] and is the same as Colella's scheme [16] on the equation studied here. We then combine this scheme with one of the second order schemes using one-dimensional Total Variation Diminishing (TVD) limiters to produce an oscillation-free scheme that is second order accurate in smooth flow. After presenting some numerical results from the two dimensional schemes, we derive the equivalent schemes in three dimensions and study their accuracy and stability.

We do not attempt to extend any schemes to nonlinear systems in this paper; such extensions are currently under development and will be the subject of future communications.

This paper is organised as follows: §2 introduces the WAF approach, and various schemes that it produces in one dimension. In §3 we consider the approach in two dimensions — we derive finite volume schemes, study their accuracy and stability, construct our oscillation free scheme and present some numerical results. In §4 we derive some three dimensional schemes. In §5 conclusions are drawn and future work is discussed.

2. The WAF approach

Consider the model hyperbolic conservation law

$$u_t + f(u)_x = 0 \qquad f(u) = au \tag{1}$$

where u is the conserved variable, $f(u)$ is the physical flux function and a is the speed of convection. We will consider schemes for (1) that are conservative time marching schemes of the form:

$$u_i^{n+1} = u_i^n - \frac{\Delta t}{\Delta x}\left[\mathbf{f}_{i+\frac{1}{2}} - \mathbf{f}_{i-\frac{1}{2}}\right] \tag{2}$$

where $\{u_i^n\}$ is a set of piecewise constant cell averages, Δt and Δx are defined as the time step size and computing cell length respectively and $\mathbf{f}_{i+\frac{1}{2}}$ is an intercell numerical flux. We define a Weighted Average Flux as:

$$\mathbf{f}_{i+\frac{1}{2}} = \frac{1}{(t_2 - t_1)}\frac{1}{(x_2 - x_1)}\int_{t_1}^{t_2}\int_{x_1}^{x_2} f(u^\star(x,t))dx\ dt \tag{3}$$

where $u^\star(x,t)$ is the solution of relevant initial value problems with data $\{u_l^n\}_{l=i-k}^{i+k+1}$. The choice of k depends on the choice of integration range in (3); this is determined by the values of x_1, x_2 and t_1, t_2.

In this section we are exclusively concerned with the choice

$$t_1 = 0 \qquad t_2 = \Delta T \qquad x_1 = -\tfrac{1}{2}\Delta x \qquad x_2 = \tfrac{1}{2}\Delta x \tag{4}$$

where ΔT could be large, that is the corresponding Courant number

$$\nu = \frac{a\Delta T}{\Delta x} \tag{5}$$

could be greater than unity. As the choice of ΔT implies a chosen Courant number, we introduce the notation $\Delta T_\nu(q_1, q_2)$ to mean that the associated Courant number ν satisfies $q_1 \le \nu \le q_2$, with q_1, q_2 non-negative real numbers.

2.1 Exact integration schemes.

Here we carry out the exact evaluation of integral (3) with choices (4) and $u^\star(x,t)$ the solution of piecewise constant Riemann problems.

First consider the case $\Delta T_\nu(0, \frac{1}{2})$. The integration range together with the relevant wave pattern is shown in Fig. 1. It is easy to see that in this case

$$\mathbf{f}_{i+\frac{1}{2}} = \frac{1}{2}(1+\nu)f_i + \frac{1}{2}(1-\nu)f_{i+1} \tag{6}$$

which is the familiar Lax-Wendroff flux for the model equation (1).

Fig. 2 shows the integration range and wave pattern for $\Delta T_\nu(\frac{1}{2}, 1)$. Exact integration produces a three point flux

$$\mathbf{f}_{i+\frac{1}{2}} = W_{-1}f_{i-1} + W_0 f_i + W_1 f_{i+1} \tag{7}$$

with

$$\left.\begin{aligned} W_{-1} &= \tfrac{1}{8\nu}(2\nu - 1)^2 \\ W_0 &= \tfrac{1}{8\nu}(-4\nu^2 + 12\nu - 2) \\ W_1 &= \tfrac{1}{8\nu} \end{aligned}\right\} \tag{8}$$

This flux in conjunction with (2) gives a second order accurate method. The case $\Delta T_\nu(1, \frac{3}{2})$ also gives the scheme (7),(8).

By performing the integration for arbitrary ΔT, we can generate an infinite sequence of schemes. The l^{th} scheme in this sequence is found by integrating with timestep $\Delta T_\nu(q_1, q_2)$ where

$$q_1 = l - \tfrac{1}{2} \quad q_2 = l + \tfrac{1}{2} \tag{9}$$

The cases $l = 0$ and $l = 1$ have been given above. Cases $l \geq 2$ can be derived similarly, and for $l \geq 4$ the intercell flux can be written in the general form

$$\mathbf{f}_{i+\frac{1}{2}} = \sum_{k=-l}^{1} W_k f_{i+k} \tag{10}$$

where

$$\begin{aligned} W_1 &= \tfrac{1}{8\nu} \\ W_0 &= \tfrac{7}{8\nu} \\ W_k &= \tfrac{1}{\nu} \qquad\qquad k \in \{2-l \ldots -1\} \\ W_{1-l} &= \tfrac{1}{\nu}\left[1 - \tfrac{1}{8}(2(\nu - l) - 1)^2\right] \\ W_{-l} &= \tfrac{1}{8\nu}(2(\nu - l) + 1)^2 \end{aligned} \tag{11}$$

2.1.1 Accuracy.

For $\Delta T_\nu(0, \frac{1}{2})$ the intercell flux (6) leads to the Lax-Wendroff method which is known to be second order accurate in space and time. For $\Delta T_\nu(\frac{1}{2}, \frac{3}{2})$ the corresponding numerical flux leads to

$$u_i^{n+1} = \sum_k b_k u_{i+k} \tag{12}$$

with

$$\left.\begin{aligned} b_{-2} &= \tfrac{1}{8}(2\nu - 1)^2 \\ b_{-1} &= \tfrac{1}{8}(-8\nu^2 + 16\nu - 3) \\ b_0 &= \tfrac{1}{8}(4\nu^2 - 12\nu + 11) \\ b_1 &= -\tfrac{1}{8} \end{aligned}\right\} \tag{13}$$

For p-th order accuracy one requires (Roe, [17])

$$\textstyle\sum_k k^q b_k = (-\nu)^q \qquad 0 \leq q \leq p \tag{14}$$

Simple manipulations show that (12),(13) is second order accurate. For the schemes $l = 2$, $l = 3$ and the general scheme with intercell flux (10), (11) second order accuracy also follows from (14).

2.1.2 Stability.

The scheme $l = 0$ is the Lax-Wendroff scheme, and it is well known that this is stable provided $\nu \leq 1$. We have not managed to formally derive stability limits for any cases $l \geq 1$; however plotting the von Neumann amplification factor for various schemes in the sequence, at various Courant numbers, suggests that the lth scheme, $l \geq 1$, is stable whenever

$$l - \frac{1}{\sqrt{2}} \leq \nu \leq l + \frac{1}{\sqrt{2}} \tag{15}$$

2.2 Approximate integration schemes.

Formula (3) with restriction (4) becomes

$$\mathbf{f}_{i+\frac{1}{2}} = \frac{1}{\Delta T}\frac{1}{\Delta x}\int_0^{\Delta T}\int_{-\frac{1}{2}\Delta x}^{\frac{1}{2}\Delta x} f(u^\star(x,t))\, dx\, dt \tag{16}$$

We now study schemes that can be generated from this general flux if approximate integration methods are used.

2.2.1 The midpoint rule in space.

Use of the midpoint rule in space gives

$$\mathbf{f}_{i+\frac{1}{2}} = \frac{1}{\Delta T}\int_0^{\Delta T} f(u^\star(0,t))dt \tag{17}$$

which is the usual time-average intercell flux evaluation along the t-axis in the solution of the Riemann problem. If $u^\star(x,t)$ is taken to represent the solution of the conventional **piecewise constant Riemann problem** (CRP) with data u_i^n, u_{i+1}^n then the first order Godunov method is reproduced. Equation (17) gives

$$\mathbf{f}_{i+\frac{1}{2}} = \begin{cases} au_i & \text{if } a > 0 \\ au_{i+1} & \text{if } a < 0 \end{cases} \tag{18}$$

If $u^\star(x,t)$ in (17) is taken to represent the solution of a **generalised Riemann problem** with piecewise linear data

$$u_i(x) = u_i^n + (x - x_i)\tfrac{\Delta i}{\Delta x} \quad x \in [0, \Delta x] \tag{19}$$

with the slope Δi defined as

$$\Delta i = \alpha(u_i - u_{i-1}) + (1-\alpha)(u_{i+1} - u_i) \tag{20}$$

then the midpoint rule in time applied to (17) gives:

$$\mathbf{f}_{i+\frac{1}{2}} = a\left[u_i^n + \frac{1}{2}(1-\nu)\Delta i\right] \tag{21}$$

This result is obtained by finding the exact solution for $\frac{1}{2}\Delta t$. For $a > 0$ this is

$$u_i(x^\star) = u_i^n + \frac{1}{2}(1-\nu)\Delta i \tag{22}$$

where $x^* = (1 - \frac{1}{2}\nu)\Delta x$. Substitution of Δi into (21) gives

$$\mathbf{f}_{i+\frac{1}{2}} = W_{-1} f_{i-1} + W_0 f_i + W_1 f_{i+1} \tag{23}$$

Table 1 shows some well known schemes derived from (23).

	W_1	W_2	W_3	Scheme
α	$-\frac{1}{2}(1-\nu)\alpha$	$1+\frac{1}{2}(1-\nu)(2\alpha-1)$	$\frac{1}{2}(1-\nu)(1-\alpha)$	
0	0	$\frac{1}{2}(1+\nu)$	$\frac{1}{2}(1-\nu)$	Lax-Wendroff
$\frac{1}{2}$	$-\frac{1}{4}(1-\nu)$	1	$\frac{1}{4}(1-\nu)$	Fromm
1	$\frac{1}{2}(\nu-1)$	$\frac{1}{2}(3-\nu)$	0	Warming-Beam

Table 1

All schemes listed in Table 1 are second-order accurate, including the general α scheme; by using (14) this leads to a third order accurate scheme for the particular choice $\alpha = \frac{1}{3}(1+\nu)$.

The same result (23) can be obtained using the Generalised Riemann Problem (GRP) approach of Ben-Artzi and Falcovitz [8], whereby a flux is defined as:

$$\mathbf{f}_{i+\frac{1}{2}} = f(u_{i+\frac{1}{2}}^{n+\frac{1}{2}}) \tag{24}$$

with $u_{i+\frac{1}{2}}^{n+\frac{1}{2}}$ obtained from a Taylor series expansion

$$u_{i+\frac{1}{2}}^{n+\frac{1}{2}} = u^{(0)} + \frac{1}{2}\Delta t \frac{\delta}{\delta t} u^{(0)} \tag{25}$$

where $u^{(0)}$ is the solution to the conventional Riemann problem with data u_i^R, u_{i+1}^L, the right and left extrapolated values obtained from (19). Use of (1) gives $u_t = -a u_x$ which, if substituted into (25) gives a numerical flux equivalent to (23). Thus the GRP method could be interpreted as a special case of the WAF approach with midpoint rule integration to evaluate (17).

Also, the well known PLM method [7] falls within this category. Use of the trapezium rule to evaluate (17) gives:

$$\mathbf{f}_{i+\frac{1}{2}} = \frac{1}{2}\left[f(u^{(0)}) + f(u^{(1)})\right] \tag{26}$$

where u^0 is as in (25) and $u^{(1)}$ is the solution $u^*(0, \Delta t)$ at the complete time level. This is found by evaluating (for $a > 0$) $u_i(x)$ in (19) at $x = (1-\nu)\Delta x$, namely

$$u^{(1)} = u_i^n + \left(\frac{1}{2} - \nu\right)\Delta i \tag{27}$$

Substitution of (27) into (26) gives the intercell flux (23) that reproduces the second order schemes listed in Table 1.

As a matter of fact, exact time integration also gives the same scheme (23); $u^\star(0,t)$ is linear in time and so both the midpoint rule and trapezium rule are exact.

2.2.2 Approximations in time.

A midpoint rule in time applied to (16) gives

$$\mathbf{f}_{i+\frac{1}{2}} = \frac{1}{\Delta x}\int_{-\frac{1}{2}\Delta x}^{\frac{1}{2}\Delta x} f(u^\star(x, \frac{1}{2}\Delta t))dx \tag{28}$$

Here assume $u^\star$ is the exact solution of the piecewise constant Riemann problem. Exact space integration gives

$$\mathbf{f}_{i+\frac{1}{2}} = \frac{1}{2}(1+\nu)f_i + \frac{1}{2}(1-\nu)f_{i+1} \tag{29}$$

when $0 \le \nu \le 1$, which is again the Lax-Wendroff flux for (1). This was observed by Toro [10]. For $1 \le \nu \le 2$ exact integration in (28) gives

$$\mathbf{f}_{i+\frac{1}{2}} = \frac{1}{2}(\nu-1)f_{i-1} + \frac{1}{2}(3-\nu)f_i \tag{30}$$

which is the flux for the Warming and Beam second order upwind method [18]. This is stable provided $0 \le \nu \le 2$.

2.3 Large timestep schemes.

For the time-dependent, one-dimensional equation (1) formulation (2), (4) can also provide stable, "large timestep" schemes. This is achieved by selecting a large timestep $\Delta t_\nu(q_1, q_2)$ with $q_2 \ge 1$. Exact integration schemes with large Δt were derived in §2.1. Approximate integration schemes were first tried by Casulli and Toro [19]. They derived second order TVD schemes for the linear advection equation (1) with arbitrary, large timestep Δt. The extension of the schemes to linear systems with constant coefficients is trivial. Toro and Billett [20], [21] have studied the extension of schemes with fluxes (29) and (30) for timesteps $\Delta t_\nu(q_1, q_2)$ with $q_1 = 0$, $q_2 = 2$. The technique has been applied to the time-dependent, two dimensional Euler equations. Although successful, the efficiency gains of this scheme are still modest, as the maximum Courant number is two. More ambitious extensions are currently being investigated. They involve front-tracking and local adaptivity ideas.

3. Application in two space dimensions

In this section we show how the WAF approach, as discussed in the last section, can be used to generate two-dimensional finite volume schemes. Our aim is to illustrate the approach, rather than provide an exhaustive account of all possibilities. Therefore, after defining an intercell flux for the general case, we restrict ourselves to the regular, Cartesian grids, assume the data is constant within each cell and consider only Courant numbers less than unity. Applications to curvilinear or unstructured grids are, of course, also possible, as well as GRP or MUSCL type schemes, and 'large timestep' schemes when the Courant numbers are greater than unity, but we do not consider these here.

We will first consider the constant wave speed case and explore the schemes that can be generated from combinations of exact integration and the midpoint rule in space and time. We

study their accuracy and stability. We then show how two of the schemes can be combined to give a monotone scheme that is second order accurate in regions of smooth flow, and generalise the scheme to the variable wavespeed case. Some numerical results will then be presented.

In two space dimensions the linear advection equation can be written as

$$u_t + f_x + g_y = 0 \tag{31}$$

where $f = au$ and $g = bu$ are flux components, a and b are speeds of propagation, and (x, y) are two space coordinates.

For a general grid (structured or unstructured), we can define a general WAF intercell flux $\mathbf{e}_{AB}$ for boundary AB as

$$\mathbf{e}_{AB} = \frac{1}{t_2 - t_1}\frac{1}{V(I)}\int_{t_1}^{t_2}\int_I \mathbf{e}\cdot\mathbf{n}\, dx\, dy\, dt \tag{32}$$

where I is a space integration range in (x, y), $V(I)$ is the area of I, $\mathbf{e} = (au, bu)$ is the general flux function, and $\mathbf{n}$ is the unit outward facing vector normal to the intercell boundary. See Fig. 3.

3.1 Multidimensional schemes for Cartesian grids

We consider here the simple case of regular Cartesian grids. Let Δx, Δy be the mesh spacing, Δt be the timestep and assume that a and b are constant and positive, unless otherwise stated. Consider the two dimensional conservation formula

$$u_{i,j}^{n+1} = u_{i,j}^n - \frac{\Delta t}{\Delta x}\left[\mathbf{f}_{i+\frac{1}{2},j} - \mathbf{f}_{i-\frac{1}{2},j}\right] - \frac{\Delta t}{\Delta y}\left[\mathbf{g}_{i,j+\frac{1}{2}} - \mathbf{g}_{i,j-\frac{1}{2}}\right] \tag{33}$$

where $u_{i,j}^n$ is the integral average of u in cell (i, j) at time level n and $\mathbf{f}_{i+\frac{1}{2},j}$ and $\mathbf{g}_{i,j+\frac{1}{2}}$ are intercell fluxes in the x and y directions respectively. When applied to Cartesian grids, the formula (32) gives intercell fluxes in the x-direction as

$$\mathbf{f}_{i+\frac{1}{2},j} = \frac{1}{t_2 - t_1}\frac{1}{V(I)}\int_{t_1}^{t_2}\int_I f(u^\star(x, y, t))dx\, dy\, dt \tag{34}$$

where $u^\star(x, y, t)$ is the solution to the initial value problem defined by (31) with initial data u^n at time level n. The fluxes in the y-direction follow by symmetry. Define the Courant numbers in the x and y directions as $\nu_x = a\frac{\Delta t}{\Delta x}$ and $\nu_y = b\frac{\Delta t}{\Delta y}$ respectively. We consider here only the case when the time limits are $t_1 = 0$ and $t_2 = \Delta t$, where Δt is the timestep chosen such that $\nu_x \leq 1$ and $\nu_y \leq 1$. For the flux $\mathbf{f}_{i+\frac{1}{2},j}$ we always take the space integration range as:

$$I = \left[-\frac{1}{2}\Delta x, \frac{1}{2}\Delta x\right] \times [0, \Delta y] \tag{35}$$

where, in local coordinates, $x = 0$ lie on the boundary, and $y = 0$, $y = \Delta y$ lie on the ends on the boundary. For the flux $\mathbf{g}_{i,j+\frac{1}{2}}$ the obvious changes are made. See Fig. 4.

This choice of Courant numbers and integration range restricts the number of states that influence $\mathbf{f}_{i+\frac{1}{2},j}$ to four: $u_{i,j}^n$, $u_{i+1,j}^n$, $u_{i,j-1}^n$ and $u_{i+1,j-1}^n$. These are laid out in the four quadrants of a square, and form the initial conditions of a two dimensional Riemann problem.

3.1.1 Exact integration in all directions

Consider first the case of exact integration in time and both space directions. We assume that $\nu_x \leq \frac{1}{2}$ and $\nu_y \leq \frac{1}{2}$ to restrict the number of waves entering the integration range. The evaluation of the integral (34) is, infact, not as hard as it might seem: we know the exact solution to the two dimensional Riemann problem for (31) at any time, with any states in the four quadrants. The equation simply advects the given initial conditions in the direction specified by a and b. See Fig. 5. The point A moves to the point A_2. The point B moves out of the integration range. At any given point (x, y) in I, and at any $t \in [t_1, t_2]$, we know the value of the flux $f = au$. To obtain our intercell flux, we integrate these fluxes through space and time. This gives the intercell flux $\mathbf{f}_{i+\frac{1}{2},j}$ as:

$$\begin{aligned}\mathbf{f}_{i+\frac{1}{2},j} &= \frac{1}{12}\left[6 + 6\nu_x - 3\nu_y - 4\nu_x\nu_y\right] f_{i,j} + \frac{1}{12}\left[6 - 6\nu_x - 3\nu_y + 4\nu_x\nu_y\right] f_{i+1,j} \\ &+ \frac{1}{12}\left[3\nu_y + 4\nu_x\nu_y\right] f_{i,j-1} + \frac{1}{12}\left[3\nu_y - 4\nu_x\nu_y\right] f_{i+1,j-1} \end{aligned} \tag{36}$$

where $f_{i,j} = f(u^n_{i,j}) = au^n_{i,j}$. The intercell flux $\mathbf{g}_{i,j+\frac{1}{2}}$ follows by symmetry. Substituting both $\mathbf{f}_{i+\frac{1}{2},j}$ and $\mathbf{g}_{i,j+\frac{1}{2}}$ into the conservative formula (33) gives the full scheme as:

$$\begin{aligned} u^{n+1}_{i,j} &= \left[1 - \nu_x^2 - \nu_y^2 + \frac{2}{3}\nu_x\nu_y(\nu_x + \nu_y)\right] u^n_{i,j} \\ &+ \frac{1}{12}\nu_y\left[6(\nu_y - 1) + \nu_x(3 - 4\nu_y)\right] u^n_{i,j+1} \\ &+ \frac{1}{12}\nu_x\left[6(\nu_x - 1) + \nu_y(3 - 4\nu_x)\right] u^n_{i+1,j} \\ &+ \frac{1}{12}\nu_x\nu_y(4\nu_x - 3)u^n_{i+1,j-1} + \frac{1}{12}\nu_x\nu_y(4\nu_y - 3)u^n_{i-1,j+1} \\ &+ \frac{1}{12}\nu_y\left[6(1 + \nu_y) - \nu_x(3 + 4\nu_y + 8\nu_x)\right] u^n_{i,j-1} \\ &+ \frac{1}{12}\nu_x\left[6(1 + \nu_x) - \nu_y(3 + 4\nu_x + 8\nu_y)\right] u^n_{i-1,j} \\ &+ \frac{1}{12}\nu_x\nu_y\left[6 + 4(\nu_x + \nu_y)\right] u^n_{i-1,j-1} \end{aligned} \tag{37}$$

This scheme has an eight point stencil with both upwind and downwind components, as shown in Fig. 6. A truncation error analysis shows this scheme to be second order accurate in space and time. Note that when $\nu_x = 0$ or $\nu_y = 0$, the scheme reduces to the one dimensional Lax-Wendroff scheme. Scheme (37) appears to be new.

3.1.2 The midpoint rule in space

We now consider the schemes generated by using exact integration in time and the midpoint rule in space in (34). We again assume that $\nu_x \leq \frac{1}{2}$ and $\nu_y \leq \frac{1}{2}$. There are three cases to consider: (i) the midpoint rule parallel to the boundary, and exact integration perpendicular to the boundary; (ii) the midpoint rule perpendicular to the boundary, and exact integration parallel to the boundary; (iii) the midpoint rule in both directions.

(i) *The midpoint rule parallel to the boundary*

Here we consider exact integration in time, the midpoint rule parallel to the boundary, and exact integration perpendicular to the boundary. The integral form of the intercell flux (34) in this case is:

$$\mathbf{f}_{i+\frac{1}{2},j} = \frac{1}{\Delta t}\frac{1}{\Delta x}\int_0^{\Delta t}\int_{I\bigcap\{y=\frac{1}{2}\Delta y\}} f(u^*(x,\frac{1}{2}\Delta y,t))\,dx\,dt \tag{38}$$

where we integrate over the plane $y = \frac{1}{2}\Delta y$. See Fig. 7a. This gives the intercell flux $\mathbf{f}_{i+\frac{1}{2},j}$ as:

$$\mathbf{f}_{i+\frac{1}{2},j} = \frac{1}{2}(1+\nu_x)f_{i,j} + \frac{1}{2}(1-\nu_x)f_{i+1,j} \tag{39}$$

This is the flux for the finite volume **WAF** scheme put forward by Speares [22]. This is the one-dimensional **WAF** flux and would be the most obvious finite volume extension. However, it has been proved to be second order accurate only when the flow is aligned to the grid. In §3.1.5 we demonstrate that it is also linearly unstable without this restriction on the flow.

(ii) *The midpoint rule perpendicular to the boundary*

Here we consider exact integration in time, the midpoint rule perpendicular to the boundary, and exact integration parallel to the boundary. The integral form of the intercell flux (34) simplifies in this case to:

$$\mathbf{f}_{i+\frac{1}{2},j} = \frac{1}{\Delta t}\frac{1}{\Delta y}\int_0^{\Delta t}\int_{I\bigcap\{x=0\}} f(u^*(0,y,t))\,dy\,dt \tag{40}$$

where we integrate over the plane $x = 0$. See Fig. 7b. This gives the intercell flux $\mathbf{f}_{i+\frac{1}{2},j}$ as:

$$\mathbf{f}_{i+\frac{1}{2},j} = \frac{1}{2}(2-\nu_y)f_{i,j} + \frac{1}{2}\nu_y f_{i,j-1} \tag{41}$$

The scheme resulting from this flux is:

$$\begin{aligned} u_{i,j}^{n+1} &= (1-\nu_x-\nu_y+\nu_x\nu_y)u_{i,j}^n + \nu_y(1-\nu_x)u_{i,j-1}^n \\ &\quad +\nu_x(1-\nu_y)u_{i-1,j}^n + \nu_x\nu_y u_{i-1,j-1}^n \end{aligned} \tag{42}$$

It can be shown to be first order accurate and is identical to the first order multidimensional upwind scheme of Colella [16] on the linear equation (31).

(iii) *The midpoint rule in both directions*

Here we consider exact integration in time, and the midpoint rule in both space directions. The integral form of the intercell flux (34) simplifies in this case to:

$$\mathbf{f}_{i+\frac{1}{2},j} = \frac{1}{\Delta t}\int_0^{\Delta t} f(u^*(0,\frac{1}{2}\Delta y,t))\,dt \tag{43}$$

i.e we integrate along the line $x = 0$, $y = \frac{1}{2}\Delta y$. See Fig. 7c. This gives the intercell flux $\mathbf{f}_{i+\frac{1}{2},j}$ as:

$$\mathbf{f}_{i+\frac{1}{2},j} = f_{i,j} \tag{44}$$

This is simply a finite volume version of Godunov's method. It is known to be first order accurate.

3.1.3 The midpoint rule in time

We now consider the midpoint rule in time combined with exact integration in both space directions and assume that $\nu_x \leq 1$ and $\nu_y \leq 1$. The integral form of the intercell flux (34) simplifies in this case to:

$$\mathbf{f}_{i+\frac{1}{2},j} = \frac{1}{\Delta x \Delta y} \int_I f(u^\star(x, y, \frac{1}{2}\Delta t))\, dx\, dy \tag{45}$$

i.e we integrate over the plane $t = \frac{1}{2}\Delta t$. See Fig. 8. This gives intercell flux:

$$\begin{aligned} \mathbf{f}_{i+\frac{1}{2},j} &= \frac{1}{4}(1+\nu_x)(2-\nu_y) f_{i,j} + \frac{1}{4}(1-\nu_x)(2-\nu_y) f_{i+1,j} \\ &\quad + \frac{1}{4}(1+\nu_x)\nu_y f_{i,j-1} + \frac{1}{4}(1-\nu_x)\nu_y f_{i+1,j-1} \end{aligned} \tag{46}$$

The flux $\mathbf{g}_{i,j+\frac{1}{2}}$ follows similary. Substituting both fluxes into the conservative scheme (33) gives the scheme in full form as:

$$\begin{aligned} u_{i,j}^{n+1} &= \left[1 - \frac{1}{2}\nu_x^2(2-\nu_y) - \frac{1}{2}\nu_y^2(2-\nu_x)\right] u_{i,j}^n \\ &\quad - \frac{1}{4}\nu_x(1-\nu_x)(2-\nu_y) u_{i+1,j}^n - \frac{1}{4}(2-\nu_x)\nu_y(1-\nu_y) u_{i,j+1}^n \\ &\quad - \frac{1}{4}\nu_x\nu_y(1-\nu_x) u_{i+1,j-1}^n - \frac{1}{4}\nu_x\nu_y(1-\nu_y) u_{i-1,j+1}^n \\ &\quad + \frac{1}{4}\left[\nu_x(1+\nu_x)(2-\nu_y) - 2\nu_x\nu_y^2\right] u_{i-1,j}^n + \frac{1}{4}\left[\nu_y(1+\nu_y)(2-\nu_x) - 2\nu_x^2\nu_y\right] u_{i,j-1}^n \\ &\quad + \frac{1}{4}\nu_x\nu_y(2+\nu_x+\nu_y) u_{i-1,j-1}^n \end{aligned} \tag{47}$$

Note that the scheme has the eight point compact stencil shown in Fig. 6. A truncation error analysis shows the scheme to be second order accurate in space and time. Note that when $\nu_x = 0$ or $\nu_y = 0$, the scheme reduces to the one dimensional Lax-Wendroff scheme, and that when $\nu_x = \nu_y = 1$, the scheme reduces to

$$u_{i,j}^{n+1} = u_{i-1,j-1}^n \tag{48}$$

which reproduces the exact solution under the given initial conditions. To our knowledge, the scheme (47) is new.

3.1.4 The midpoint rule in both space and time

We now consider the schemes generated by using the midpoint rule in time and combinations of exact integration and the midpoint rule in space. We again assume that $\nu_x \leq 1$ and $\nu_y \leq 1$. As in §3.1.2, there are three cases to consider: (i) the midpoint rule parallel to the boundary and exact integration perpendicular to the boundary; (ii) the midpoint rule perpendicular to

the boundary and exact integration parallel to the boundary; (iii) the midpoint rule in both directions. In cases (i) and (ii), the integral is an integral in two dimensions: one space dimension, where exact integration is used, and one in time, where the midpoint rule is use. Recall from §2 that in this situation, the resulting scheme is the same as when exact integration in time is used. The same result holds for (iii). Thus the three cases here will result in the same schemes as cases (i), (ii), (iii) in §3.1.2

3.1.5 Stability

We have not managed to perform rigorous stability analysis on any of the schemes presented in this section. However, a good indication of the stability of a scheme can be found by computing the von Neumann amplification coefficient A for a large number of quadruples $(\nu_x, \nu_y, \theta, \phi)$, where θ and ϕ are the phase angles in the x and y directions respectively. We can define $st(\nu_x, \nu_y)$ to be the ratio of stable pairs (θ, ϕ) for given (ν_x, ν_y), i.e the number for which $\mid A \mid \leq 1$, to the total number tested. The scheme is only stable for the pair (ν_x, ν_y) if $st(\nu_x, \nu_y) = 1$, i.e all Fourier modes are stable. Fig. 9 shows contour plots of $st(\nu_x, \nu_y)$ against (ν_x, ν_y) when $\nu_x \leq 2$ and $\nu_y \leq 2$ for four of the schemes derived in this section.

Fig 9a is the plot for the scheme (37) derived using exact integration in all directions in §3.1.1. It suggests that the scheme is stable whenever

$$\sqrt{(\nu_x^2 + \nu_y^2)} \leq 1 \tag{49}$$

Recall that the scheme is also second order accurate in space and time, and thus a two-dimensional extension of the Lax-Wendroff scheme. It is much more stable than the "traditional" Lax-Wendroff schemes in two dimensions, which are restricted by the condition

$$\sqrt{(\nu_x^2 + \nu_y^2)} \leq \frac{1}{\sqrt{8}} \tag{50}$$

See Hirsch [23]

Fig 9b is the plot for the scheme with flux (39) derived in §3.1.2.(i) using exact integration in time and perpendicular to the boundary, and the midpoint rule parallel to the boundary. It shows the scheme to be unstable unless the flow is aligned to the grid, when the appropriate Courant number must be less than unity. The lack of stability of this scheme is due to the fact that it does not take into account the multidimensional nature of the problem.

Fig 9c is the plot for the first order scheme (41) derived using exact integration in time, exact integration parallel to the boundary, and the midpoint rule perpendicular to the boundary in §3.1.2. As mentioned before, it is Colella's scheme [16]. It shows the scheme to be stable whenever

$$\max\{\nu_x, \nu_y\} \leq 1 \tag{51}$$

Colella proved this condition analytically.

Fig 9d is the plot for the second order accurate scheme (47) derived using the midpoint rule in time, and exact integration in both space dimensions in §3.1.3. It shows the scheme also has the stability condition (51).

A plot of the function $st(\nu_x, \nu_y)$ for the scheme with flux (44), i.e the finite volume Godunov scheme, is not shown. The scheme is stable provided

$$\nu_x + \nu_y \leq 1 \tag{52}$$

This is a well known result.

3.2 Ān oscillation-free finite volume method for two space dimensions

We now construct an oscillation-free, finite volume scheme that is second order accurate in space and time in regions of smooth flow. We use two of the methods derived in the last section: the second order scheme (47) and the first order scheme (43). We choose these because (47) can be broken down into a useful wave model, and linked to (43) to produce an oscillation-free method in a very simple way. It happens that these schemes are also the most stable two-dimensional schemes of those presented so far in this paper.

Consider the second order scheme (47). This has intercell flux

$$\begin{aligned}\mathbf{f}_{i+\frac{1}{2},j} &= \frac{1}{4}(1+\nu_x)(2-\nu_y)f_{i,j} + \frac{1}{4}(1-\nu_x)(2-\nu_y)f_{i+1,j} \\ &+\frac{1}{4}(1+\nu_x)\nu_y f_{i,j-1} + \frac{1}{4}(1-\nu_x)\nu_y f_{i+1,j-1}\end{aligned} \tag{53}$$

We wish to write this flux as a weighted sum of flux jumps across waves from one-dimensional, grid-aligned Riemann problems at nearby intercell boundaries. This will enable us to extend the scheme to the case when the the wavespeeds a and b vary in space and time later in this section, and to non-linear systems in future communications. Since $a > 0$, $b > 0$ and $\nu_x \leq 1$, $\nu_y \leq 1$ there will be just four boundaries involved, labeled as in Fig. 10. The form in which we need the flux is therefore:

$$\mathbf{f}_{i+\frac{1}{2},j} = \frac{1}{2}(f_{i,j} + f_{i+1,j}) - \frac{1}{2}\sum_{l=1}^{4}\eta_l \Delta f^l \tag{54}$$

We wish to solve for the coefficients η in (54), but there is only a unique solution for certain *differences* in these coefficients, not the coefficient themselves. However, we can choose a sensible set $\{\eta\}$ as follows.

Consider a wave from any grid aligned Riemann problem. It will have a component of velocity perpendicular to the boundary at which it was generated. This velocity is the wavespeed from the solution to the Riemann problem at that boundary, and always equals the constant speed a in the present case. We can make the wave truly two dimensional by also giving it a component of velocity parallel to the boundary. For this velocity, we simply take the component of velocity parallel to the boundary from the cell into which the wave is propagating. This will always be the constant b in the present case. With these two components of velocity, the wave will sweep over an area in space as time progresses. See Fig. 11. Recall the scheme was originally derived via the midpoint rule in time. At time $t = \frac{1}{2}\Delta t$, part (or all) of this area will intersect the space integration range I defined earlier. We set the weight η for each wavejump in (55) equal to the area of this intersection divided by the area of the space integration range. Thus (54) becomes:

$$\begin{aligned}\mathbf{f}_{i+\frac{1}{2},j} = \tfrac{1}{2}(f_{i,j} + f_{i+1,j}) - \tfrac{1}{8}\nu_x\nu_y(f_{i+1,j-1} - f_{i,j-1}) - \tfrac{1}{8}(2+\nu_x)\nu_y(f_{i,j} - f_{i,j-1}) \\ -\tfrac{1}{8}(2-\nu_x)\nu_y(f_{i+1,j} - f_{i+1,j-1}) - \tfrac{1}{8}\nu_x(4-\nu_y)(f_{i+1,j} - f_{i,j})\end{aligned} \tag{55}$$

and (54) is now in the required form. The fluxes $\mathbf{g}_{i,j+\frac{1}{2}}$ can be treated in a similar manner. In the linear problem we are now studying, the wave model described here is essentially the same as the wave model of LeVeque [24]. The authors are developing the scheme (47) to non-linear systems using this wave model.

The scheme (55), being second order accurate, will suffer from oscillations in regions of high gradients. These are unphysical, and therefore undesirable. In one space dimension, one way to overcome this problem and maintain second order accuracy in smooth flow is to design schemes

that satisfy certain Total Variation Diminishing (TVD) criteria. We do not discuss details of this here, but refer the reader to the work of Harten [25]. Schemes can be made TVD by introducing limiter functions (Sweby [26]) that preserve second order terms in the scheme when it is safe to do so.

The WAF method applied to the linear advection equation in one space dimension has intercell flux

$$\mathbf{f}_{i+\frac{1}{2}} = \frac{1}{2}(1+\phi_{i+\frac{1}{2}})f_i + \frac{1}{2}(1-\phi_{i+\frac{1}{2}})f_{i+1} \tag{56}$$

The functions $\phi_{i+\frac{1}{2}} = \phi_{i+\frac{1}{2}}(r_{i+\frac{1}{2}}, \nu)$ are the limiters for the one dimensional WAF scheme (see Toro, [14]). When $\phi \equiv \nu$ (56) gives the intercell flux of the second order Lax-Wendroff scheme, and when $\phi \equiv 1$ it gives the intercell flux of the first order Godunov scheme, which does not suffer from unphysical oscillations. In general, the limiters depend on the (local) Courant number ν and a flow parameter $r_{i+\frac{1}{2}}$ defined as the *upwind* jump in u divided by the *local* jump in u, i.e:

$$r_{i+\frac{1}{2}} = \frac{\Delta u_{upw}}{\Delta u_{loc}} = \begin{cases} \frac{u_i - u_{i-1}}{u_{i+1} - u_i} & \text{if } \nu > 0 \\ \frac{u_{i+2} - u_{i+1}}{u_{i+1} - u_i} & \text{if } \nu < 0 \end{cases} \tag{57}$$

Two limiter functions for the WAF method are:

$$\phi(r,\nu) = \begin{cases} 1 & \text{if } r < 0 \\ 1 - (1 - \mid \nu \mid)r & \text{if } 0 < r < 1 \\ \mid \nu \mid & \text{if } r > 1 \end{cases} \tag{58}$$

and

$$\phi(r,\nu) = \begin{cases} 1 & \text{if } r < 0 \\ 1 - (1 - \mid \nu \mid)\frac{2r}{1+r} & \text{if } r > 0 \end{cases} \tag{59}$$

which are respectively related to the MINMOD and VAN LEER flux limiters.

Goodman and LeVeque [27] have shown that in two space dimensions any scheme that is strictly TVD is at most first order accurate. Since we would like to preserve the second order accuracy of the scheme (55) in regions of smooth flow, we do not attempt to construct a strictly TVD version of the scheme. However, it is possible to maintain the accuracy in smooth flow and eliminate virtually all of the oscillations in regions of high gradients by suitable use of the one dimensional WAF limiter functions. We do this by replacing the flux (55) with

$$\begin{aligned} \mathbf{f}_{i+\frac{1}{2},j} = {} & \tfrac{1}{2}(f_{i,j} + f_{i+1,j}) - \tfrac{1}{8}\phi^{(1)}_{i+\frac{1}{2},j}\nu_y(f_{i+1,j-1} - f_{i,j-1}) - \tfrac{1}{8}(2 + \phi^{(2)}_{i+\frac{1}{2},j})\nu_y(f_{i,j} - f_{i,j-1}) \\ & - \tfrac{1}{8}(2 - \phi^{(3)}_{i+\frac{1}{2},j})\nu_y(f_{i+1,j} - f_{i+1,j-1}) - \tfrac{1}{8}\phi^{(4)}_{i+\frac{1}{2},j}(4 - \nu_y)(f_{i+1,j} - f_{i,j}) \end{aligned} \tag{60}$$

where the limiter $\phi^{(l)}_{i+\frac{1}{2},j}$ is the one dimensional limiter for the contribution of boundary l ($l = 1, ..., 4$) to the flux at boundary $i + \frac{1}{2}$. Note that when $\phi^{(l)} \equiv \nu_x$ (60) reduces to (55) and is second order accurate, and when $\phi \equiv 1$ (60) reduces to (41), which is the flux for the first order oscillation-free scheme.

It was hoped that using the MINMOD or VAN LEER type limiters (58), (59) directly from the one dimensional case would ensure (60) remained oscillation-free in all situations. However, we achieved only partial success. The strategy worked well provided the flow was approximately aligned to the grid, but shocks moving oblique to the grid lines suffered from overshoots of a few

percent of shock height, though much smaller than the overshoots in the second order scheme without limiters. This problem can be greatly improved by replacing the flow parameter (57) by

$$r^{2D}_{i+\frac{1}{2},j} = (1-\nu_y) r_{i+\frac{1}{2},j} + \nu_y r_{i+\frac{1}{2},j-1} \tag{61}$$

where $r_{i+\frac{1}{2},j}$ is the one-dimensional flow parameter $r_{i+\frac{1}{2}}$ along strip j. (Recall that we are assuming $\nu_y > 0$ in the present discussion — the obvious changes must be made for $\nu_y < 0$). In most situations, this parameter appears to result in solutions without significant overshoots. There can be, however, small *undershoots* behind entropy violating shocks, upto about 1% of shock height. Better results may be obtained by further experimentation with the flow parameter.

The essential components of the scheme constructed here have been the first order scheme (43) and the second order scheme (47). These are both stable provided the condition

$$\max\{\nu_x, \nu_y\} \leq 1 \tag{62}$$

is satisfied. It is thus reasonable to assume that the scheme presented here also has this stability condition.

The extension of the scheme to the situation where a and b are variable, i.e functions of spatial position, time, and the data u is now simple. All we need do is re-define the speeds assigned to each wave in the wave model. Consider a wave propagating away from a boundary. For the speed perpendicular to the boundary, we take the wavespeed from the solution to the one-dimensional Riemann problem at that boundary. For the speed parallel to the boundary, we take the component of speed parallel to the boundary in the cell into which the wave is moving. These wavespeeds are no longer constant — they will vary in space and/or time. We then replace the Courant numbers in the weights in (55) with the local Courant numbers taken from these perpendicular and parallel velocities. The resulting intercell flux depends on wavejumps from 7 boundaries, labeled as in Fig. 12. The flux can then be written as:

$$\begin{aligned}
\mathbf{f}_{i+\frac{1}{2},j} \;=\; & \frac{1}{2}(f_{i,j} + f_{i+1,j}) \\
& -\frac{1}{8}\nu_x^{(1)} \max\{\nu_y^{(1)}, 0\}\,(f_{i+1,j-1} - f_{i,j-1}) \\
& -\frac{1}{8}(2+\nu_x^{(2)}) \max\{\nu_y^{(2)}, 0\}\,(f_{i,j} - f_{i,j-1}) \\
& -\frac{1}{8}(2-\nu_x^{(3)}) \max\{\nu_y^{(3)}, 0\}\,(f_{i+1,j} - f_{i+1,j-1}) \\
& -\frac{1}{8}\nu_x^{(4)}(4-\mid \nu_y^{(4)} \mid)\,(f_{i+1,j} - f_{i,j}) \\
& -\frac{1}{8}(2+\nu_x^{(5)}) \min\{\nu_y^{(5)}, 0\}\,(f_{i,j+1} - f_{i,j}) \\
& -\frac{1}{8}(2-\nu_x^{(6)}) \min\{\nu_y^{(6)}, 0\}\,(f_{i+1,j+1} - f_{i+1,j}) \\
& -\frac{1}{8}\nu_x^{(7)} \min\{\nu_y^{(7)}, 0\}\,(f_{i+1,j+1} - f_{i,j+1})
\end{aligned} \tag{63}$$

This scheme is limited as before by replacing each $\nu_x^{(l)}$ in (64) by a one-dimensional flux limiter

$\phi^{(l)}_{i+\frac{1}{2}}$. The flow parameter (61) must now be replaced by:

$$r^{2D}_{i+\frac{1}{2},j} = (1- \mid \nu_y \mid) r_{i+\frac{1}{2},j} + \max\{\nu_y, 0\}\ r_{i+\frac{1}{2},j-1} - \min\{\nu_y, 0\}\ r_{i+\frac{1}{2},j+1} \tag{64}$$

3.3 Numerical experiments

We now present some numerical results from the scheme developed in the last section. We first study the transport of a scalar square. We work on a square domain $[0,1]\times[0,1]$ divided into 100×100 cells. The initial conditions consist of $u = 1.0$ in the square $(x,y) \in [0.1, 0.3]\times[0.1, 0.3]$ and $u = 0.0$ elsewhere. Four cases are studied. In each case, the wavespeeds are kept constant. We set $a = 1$ and chose b such that the flow angle $\theta = \tan^{-1}(\frac{b}{a})$ to the x-direction is:

$$(i)\ \theta = 0^\circ \quad (ii)\ \theta = 15^\circ \quad (iii)\ \theta = 30^\circ \quad (iv)\ \theta = 45^\circ \tag{65}$$

Results are taken after 50 timesteps at a maximum Courant number of 0.8. We use the VAN LEER type limiter (59). Results are presented in Fig. 13a and Fig. 13b. Note that for $\theta = 0^\circ$ there is very little spreading of the solution in the y-direction. In this situation, the scheme reduces to one-dimensional WAF along each x-strip of cells. In all four cases, the results using the VAN LEER limiter have produced sharper results that the first order scheme, showing that the approach to limiting is essentially sound. Note that when the VAN LEER type limiter is used and the flow at 45° to the grid lines (Fig. 13b), an undershoot is clearly visible behind the square being advected. This is approximately 1% of shock height in magnitude.

The second problem is taken from a survey paper by Tamamidis and Assanis [28]. The domain is the square $[-4,4]\times[-4,4]$. Wavespeeds are fixed in time but vary in space according to

$$\begin{aligned} a(x,y) &= \frac{-v_t}{v_{t\ max}} \cdot \frac{y}{r} \\ b(x,y) &= \frac{v_t}{v_{t\ max}} \cdot \frac{x}{r} \end{aligned} \tag{66}$$

where $v_t = \mathrm{sech}^2(r)\tanh(r)$ is the tangential velocity around the center (0,0) and $v_{t\ max}$ is the maximum tangential velocity, set to 0.385 here. The problem has an exact analytical solution as:

$$u(x,y,t) = -\tanh\left[\frac{y}{2}\cos(\omega t) - \frac{x}{2}\sin(\omega t)\right] \tag{67}$$

where $\omega = \frac{v_t}{r v_{t max}}$ is the frequency. The initial condition u_0 is taken from (67) by setting $t = 0$ and is a function of y only. Fig. 14a shows the exact solution at times $t = 1.0$, 2.0, 3.0 and 4.0. Fig. 14b shows corresponding numerical solutions using the VAN LEER limiter. The scheme was run at a maximum Courant number of 0.8 on a grid of 100×100 cells. There is little to say, except that tiny oscillations are visible in the numerical results. These are due to the fact that the flow parameter is not properly detecting the high gradients in the flow.

4. The Three Dimensional Case

We now extend the two dimensional, oscillation-free scheme of the last section to the linear advection equation in three space dimensions:

$$u_t + a u_x + b u_y + c u_z = 0 \tag{68}$$

We assume here the wavespeeds a, b and c are constant and positive.

A general WAF intercell flux in three space dimensions can be defined in an analgous way to the two-dimensional flux (32). We define the flux $\mathbf{e}_A$ across boundary A as:

$$\mathbf{e}_A = \frac{1}{t_2 - t_1} \frac{1}{V(I)} \int_{t_1}^{t_2} \int_I \mathbf{e} \cdot \mathbf{n} \; dx \; dy \; dz \; dt \tag{69}$$

where I is the three dimensional space integration range, $V(I)$ is the volume of I, $\mathbf{e} = (au, bu, cu)$ is the general flux function and $\mathbf{n}$ is the outward facing unit vector normal to the boundary.

As in the two dimensional case, we consider the simple case of regular, Cartesian grids. Let Δx, Δy and Δz be the grid spacing, and Δt be the timestep. We use the conservative formula in the form:

$$\begin{aligned} u_{i,j,k}^{n+1} &= u_{i,j,k}^{n} - \frac{\Delta t}{\Delta x} \left[\mathbf{f}_{i+\frac{1}{2},j,k} - \mathbf{f}_{i-\frac{1}{2},j,k} \right] \\ &\quad - \frac{\Delta t}{\Delta y} \left[\mathbf{g}_{i,j+\frac{1}{2},k} - \mathbf{g}_{i,j-\frac{1}{2},k} \right] - \frac{\Delta t}{\Delta z} \left[\mathbf{h}_{i,j,k+\frac{1}{2}} - \mathbf{h}_{i,j,k-\frac{1}{2}} \right] \end{aligned} \tag{70}$$

where $\mathbf{f}_{i+\frac{1}{2},j,k}$, $\mathbf{g}_{i,j+\frac{1}{2},k}$ and $\mathbf{h}_{i,j,k+\frac{1}{2}}$ are the intercell fluxes in the x, y and z directions respectively. From (69), $\mathbf{f}_{i+\frac{1}{2},j,k}$ can be written as

$$\mathbf{f}_{i+\frac{1}{2},j,k} = \frac{1}{t_2 - t_1} \frac{1}{V(I)} \int_{t_1}^{t_2} \int_I f(u^\star(x, y, x, t)) \; dx \; dy \; dz \; dt \tag{71}$$

where $u^\star$ is the exact solution to equation (68) with the data u^n at time level n as initial conditions. The fluxes $\mathbf{g}_{i,j+\frac{1}{2},k}$ and $\mathbf{h}_{i,j,k+\frac{1}{2}}$ follow similarly. As the space integration range for $\mathbf{f}_{i+\frac{1}{2},j,k}$, we consider the natural extension of the space integration used in two dimensions, which can be written as

$$I = \left[-\frac{1}{2}\Delta x, \frac{1}{2}\Delta x \right] \times [0, \Delta y] \times [0, \Delta z] \tag{72}$$

See Fig. 15. The integration ranges for $\mathbf{g}_{i,j+\frac{1}{2},k}$ and $\mathbf{h}_{i,j,k+\frac{1}{2}}$ follow by symmetry. Define also the directional Courant numbers as $\nu_x = a\frac{\Delta t}{\Delta x}$, $\nu_y = b\frac{\Delta t}{\Delta y}$ and $\nu_z = c\frac{\Delta t}{\Delta z}$. We assume all three to be less than unity.

The choice of integration range and Courant numbers restricts the number of states influencing $\mathbf{f}_{i+\frac{1}{2},j,k}$ to a maximum of eight: $u_{i,j,k}$, $u_{i+1,j,k}$, $u_{i,j-1,k}$, $u_{i+1,j-1,k}$, $u_{i,j,k-1}$, $u_{i+1,j,k-1}$, $u_{i,j-1,k-1}$, and $u_{i+1,j-1,k-1}$ These are arranged in the eight corners of a cube, and can be considered as the initial conditions for a three dimensional Riemann problem for (68). The exact solution to this problem is known: equation (68) simply advects the initial conditions is the direction specified by a, b and c.

The second order scheme

We consider first the second order scheme. Working from the experience of the two dimensional case, we use the midpoint rule in time and exact integration in all three space directions. The flux in the x direction becomes

$$\mathbf{f}_{i+\frac{1}{2},j,k} = \frac{1}{V(I)} \int_I f(u^\star(x, y, z, \frac{1}{2}\Delta t)) \; dx \; dy \; dz \tag{73}$$

Where $u^\star$ is the exact solution of (68) with initial conditions $\{u_{i,j}^n\}$, the solution at time level n. Here we take I as the space integration range (72). Its volume is $V(I) = \Delta x \Delta y \Delta z$. This

integration range is illustrated in Fig. 16, divided into the regions occupied by different fluxes at time $\frac{1}{2}\Delta t$. Performing the integral gives the flux as:

$$\mathbf{f}_{i+\frac{1}{2},j,k} = \sum_{l,m,n} \alpha_{i+l,j+m,k+n} f_{i+l,j+m,k+n} \tag{74}$$

where the non-zero coefficients α are

$$\begin{aligned}
\alpha_{i,j,k} &= \frac{1}{8}(1+\nu_x)(2-\nu_y)(2-\nu_z) \\
\alpha_{i+1,j,k} &= \frac{1}{8}(1-\nu_x)(2-\nu_y)(2-\nu_z) \\
\alpha_{i,j-1,k} &= \frac{1}{8}(1+\nu_x)\nu_y(2-\nu_z) \\
\alpha_{i+1,j-1,k} &= \frac{1}{8}(1-\nu_x)\nu_y(2-\nu_z) \\
\alpha_{i,j,k-1} &= \frac{1}{8}(1+\nu_x)(2-\nu_y)\nu_z \\
\alpha_{i+1,j,k-1} &= \frac{1}{8}(1-\nu_x)(2-\nu_y)\nu_z \\
\alpha_{i,j-1,k-1} &= \frac{1}{8}(1+\nu_x)\nu_y\nu_z \\
\alpha_{i,j-1,k-1} &= \frac{1}{8}(1-\nu_x)\nu_y\nu_z
\end{aligned} \tag{75}$$

The fluxes $\mathbf{g}_{i,j+\frac{1}{2},k}$ and $\mathbf{h}_{i,j,k+\frac{1}{2}}$ follow by symmetry. Substituting the fluxes into the conservative formula (71) gives the final scheme as:

$$\begin{aligned}
u^{n+1}_{i,j,k} = u^n_{i,j,k} &- \frac{1}{4}\left[\nu_x^2(2-\nu_y)(2-\nu_z) + (2-\nu_x)\nu_y^2(2-\nu_z) + (2-\nu_x)(2-\nu_y)\nu_z^2)\right] u^n_{i,j,k} \\
&+ \frac{1}{8}\nu_x\left[(1+\nu_x)(2-\nu_y)(2-\nu_z) - 2\nu_y^2(2-\nu_z) - 2(2-\nu_y)\nu_z^2\right] u^n_{i-1,j,k} \\
&+ \frac{1}{8}\nu_y\left[(2-\nu_x)(1+\nu_y)(2-\nu_z) - 2\nu_x^2(2-\nu_z) - 2(2-\nu_x)\nu_z^2\right] u^n_{i,j-1,k} \\
&+ \frac{1}{8}\nu_z\left[(2-\nu_x)(2-\nu_y)(1+\nu_z) - 2(2-\nu_x)\nu_y^2 - 2\nu_x^2(2-\nu_y)\right] u^n_{i,j,k-1} \\
&+ \frac{1}{8}\nu_x\nu_y\left[(2-\nu_z)(2+\nu_x+\nu_y) - 2\nu_z^2\right] u^n_{i-1,j-1,k} \\
&+ \frac{1}{8}\nu_x\nu_z\left[(2-\nu_y)(2+\nu_x+\nu_z) - 2\nu_y^2\right] u^n_{i-1,j,k-1} \\
&+ \frac{1}{8}\nu_y\nu_z\left[(2-\nu_x)(2+\nu_y+\nu_z) - 2\nu_x^2\right] u^n_{i,j-1,k-1} \\
&+ \frac{1}{8}\nu_x\nu_y\nu_z(3+\nu_x+\nu_y+\nu_z) u^n_{i-1,j-1,k-1}
\end{aligned}$$

$$
\begin{aligned}
&- \frac{1}{8}\nu_x(1-\nu_x)(2-\nu_y)(2-\nu_z)u^n_{i+1,j,k} - \frac{1}{8}\nu_x(1-\nu_x)\nu_y(2-\nu_z)u^n_{i+1,j-1,k} \\
&- \frac{1}{8}\nu_x(1-\nu_x)(2-\nu_y)\nu_z u^n_{i+1,j,k-1} - \frac{1}{8}\nu_x(1-\nu_x)\nu_y\nu_z u^n_{i+1,j-1,k-1} \\
&- \frac{1}{8}(2-\nu_x)\nu_y(1-\nu_y)(2-\nu_z)u^n_{i,j+1,k} - \frac{1}{8}\nu_x\nu_y(1-\nu_y)(2-\nu_z)u^n_{i-1,j+1,k} \\
&- \frac{1}{8}(2-\nu_x)\nu_y(1-\nu_y)\nu_z u^n_{i,j+1,k-1} - \frac{1}{8}\nu_x\nu_y(1-\nu_y)\nu_z u^n_{i-1,j+1,k-1} \\
&- \frac{1}{8}(2-\nu_x)(2-\nu_y)\nu_z(1-\nu_z)u^n_{i,j,k+1} - \frac{1}{8}(2-\nu_x)\nu_y\nu_z(1-\nu_z)u^n_{i,j-1,k+1} \\
&- \frac{1}{8}\nu_x(2-\nu_y)\nu_z(1-\nu_z)u^n_{i-1,j,k+1} - \frac{1}{8}\nu_x\nu_y\nu_z(1-\nu_z)u^n_{i-1,j-1,k+1} \qquad (76)
\end{aligned}
$$

This scheme has a twenty point compact stencil. A truncation error analysis shows it to be second order accurate in space and time.

From the experience of the equivalent scheme in two space dimensions, we expected the stability condition for this scheme to be

$$\max\{\nu_x, \nu_y, \nu_z\} \leq 1 \qquad (77)$$

However, after computing the von-Neumann amplification coefficient at many thousands of points, it seems that this is not sufficient by itself. If we fix ν_z, we can calculate the stability function $st(\nu_x, \nu_y)$ as defined in the last section. Six of these 'slices' are shown in Fig. 17, for $\nu_z = 0.0, 0.25, 0.5, 0.75, 1.0, 1.25$. When $\nu_z = 0.0$, the scheme (76) reduces to the two dimensional scheme (47), and the stability condition is therefore the same as for that scheme in this case. However, as ν_z increases, an area around the point $\nu_x = 1$, $\nu_y = 1$ is lost to the unstable region. When $\nu_z \geq 1$, the stability region vanishes, but this was expected. We have not yet been able to work out what the exact stability region is; however, if we insist on the condition (77) and add the condition

$$\nu_x + \nu_y + \nu_z \leq 2 \qquad (78)$$

then any points satisfying both appear to be stable. We have calculated the von Neumann factor for many thousands of points within the region (77), (78) and found none to be unstable. From Fig. 17, we believe, however, that these conditions are only sufficient, and not necessary, for stability.

The first order scheme

To construct our final scheme, we need a first order scheme that is oscillation free. We now present a three dimensional version of the first order scheme (43) for the linear equation (68). This can be done be using the midpoint rule in time, the midpoint rule in space perpendicular to the boundary, and exact integration in space in both directions parallel to the boundary. See Fig. 18. The intercell flux then becomes

$$\mathbf{f}_{i+\frac{1}{2},j,k} = \frac{1}{\Delta y\ \Delta z}\int_{I\bigcap\{x=0\}} f(u(0,y,z,\frac{1}{2}\Delta t))\ dy\ dz \qquad (79)$$

This can be written explicitly as:

$$
\begin{aligned}
\mathbf{f}_{i+\frac{1}{2},j,k} \quad = \quad & \frac{1}{4}(2-\nu_y)(2-\nu_z)f_{i,j,k} + \frac{1}{4}\nu_y(2-\nu_z)f_{i,j-1,k} \\
& + \frac{1}{4}(2-\nu_y)\nu_z f_{i,j,k-1} + \frac{1}{4}\nu_y\nu_z f_{i,j-1,k-1}
\end{aligned} \qquad (80)
$$

The other fluxes, $\mathbf{g}_{i,j+\frac{1}{2},k}$ and $\mathbf{h}_{i,j,k+\frac{1}{2}}$, follow by symmetry. Substituting these into the conservative formula (71) gives the scheme in its full form as:

$$\begin{aligned}
u^{n+1}_{i,j,k} &= \left[1-\frac{1}{4}\nu_x(2-\nu_y)(2-\nu_z)-\frac{1}{4}(2-\nu_x)\nu_y(2-\nu_z)-\frac{1}{4}(2-\nu_x)(2-\nu_y)\nu_z\right]u^n_{i,j,k} \\
&+\nu_x\left[(1-\nu_y)(1-\nu_z)-\frac{1}{4}\nu_y\nu_z\right]u^n_{i-1,j,k}+\frac{1}{4}(4-3\nu_x)\nu_y\nu_z u^n_{i,j-1,k-1} \\
&+\nu_y\left[(1-\nu_x)(1-\nu_z)-\frac{1}{4}\nu_x\nu_z\right]u^n_{i,j-1,k}+\frac{1}{4}\nu_x(4-3\nu_y)\nu_z u^n_{i-1,j,k-1} \\
&+\nu_z\left[(1-\nu_x)(1-\nu_y)-\frac{1}{4}\nu_x\nu_y\right]u^n_{i,j,k-1}+\frac{1}{4}\nu_x\nu_y(4-3\nu_z)u^n_{i-1,j-1,k} \\
&+\frac{3}{4}\nu_x\nu_y\nu_z u^n_{i-1,j-1,k-1}
\end{aligned} \tag{81}$$

This scheme is first order accurate, and has the same stability region as the second order scheme presented above.

Wave decomposition of the second order scheme

We now show how the second order scheme can be decomposed in central differencing plus a sum of flux jumps from nearby boundaries. We want to write the flux (74,75) in the form

$$\mathbf{f}_{i+\frac{1}{2},j,k}=\frac{1}{2}(f_{i,j,k}+f_{i+1,j,k})-\sum_{l=1,12}\zeta_l\Delta f^l \tag{82}$$

where Δf^l is the flux jump across the lth boundary and ζ_l is the corresponding coefficient. There are twelve boundaries involved in the present case (constant, positive wavespeeds) which we label as in Fig. 19. If we write the flux (82) out in full and compare it with (74,75), we find we have eight conditions (from enforcing equality of coefficients) governing twelve "variables" (the coefficients ζ_l). The the set of possible coefficients $\{\zeta_l\}$ is therefore not unique. To choose a set of coefficients we look back at the two dimensional case. Recall that the weight for each boundary equalled the area of the intersection of the integration range with the region swept out by a wave from that boundary at time $t=\frac{1}{2}\Delta t$ divided by the area of the integration range. To calculate the weights ζ_l for the 3D case, we therefore apply the equivalent principle, except, of course, using *volumes* instead of *areas* — each weight should be the volume of the intersection of the integration range with the region swept out by the wave from the boundary at time $t=\frac{1}{2}\Delta t$ divided by the volume of the integration range. As an example, Fig. 20 shows the intersection of the volume swept out by the wave from boundary 1 with the integration range. The coefficients derived via this approach are:

$$\begin{aligned}
\zeta_1 &= \frac{1}{24}\nu_x(12-3\nu_y-3\nu_z+\nu_y\nu_z) \\
\zeta_2 &= \frac{1}{48}\nu_y(12+6\nu_x-3\nu_z-2\nu_x\nu_y) \\
\zeta_3 &= \frac{1}{48}\nu_y(12-6\nu_x-3\nu_z+2\nu_x\nu_z) \\
\zeta_4 &= \frac{1}{24}\nu_x\nu_y(3-\nu_z)
\end{aligned}$$

$$
\begin{aligned}
\zeta_5 &= \frac{1}{24}\nu_x\nu_z(3-\nu_y) \\
\zeta_6 &= \frac{1}{48}\nu_y\nu_z(3+2\nu_x) \\
\zeta_7 &= \frac{1}{48}\nu_y\nu_z(3-2\nu_x) \\
\zeta_8 &= \frac{1}{24}\nu_x\nu_y\nu_z \\
\zeta_9 &= \frac{1}{48}\nu_z(12-6\nu_x-3\nu_y+2\nu_x\nu_y) \\
\zeta_{10} &= \frac{1}{48}\nu_z(12+6\nu_x-3\nu_y-2\nu_x\nu_y) \\
\zeta_{11} &= \frac{1}{48}\nu_y\nu_z(3+2\nu_x) \\
\zeta_{12} &= \frac{1}{48}\nu_y\nu_z(3-2\nu_x)
\end{aligned}
\tag{83}
$$

In the general case (variable wavespeeds of any sign) there would be 23 boundaries involved. We do not discuss this here, since it follows easily from the two dimensional case.

Removing oscillations

The second order scheme can be made virtually oscillation-free by taking the flux (82) and replacing each ν_x by a one-dimensional limiter ϕ, as we did in the two dimensional case. Similarly for $\mathbf{g}_{i,j+\frac{1}{2},k}$ and $\mathbf{h}_{i,j,k+\frac{1}{2}}$. The flow parameter will again have to be replaced by a more multi-dimensional flow parameter. The natural extension of the flow parameter used in the one dimensional case would be:

$$
\begin{aligned}
r^{3D}_{i+\frac{1}{2},j,k} &= (1-\nu_y)(1-\nu_z)r_{i+\frac{1}{2},j,k} + (1-\nu_y)\nu_z r_{i+\frac{1}{2},j,k-1} \\
&\quad +\nu_y(1-\nu_z)r_{i+\frac{1}{2},j-1,k} + \nu_y\nu_z r_{i+\frac{1}{2},j-1,k-1}
\end{aligned}
\tag{84}
$$

where $r_{i+\frac{1}{2},j,k}$ is the one-dimensional flow parameter $r_{i+\frac{1}{2}}$ defined by (57) along the one dimensional strip (j,k). Other choices are, of course, possible.

Summary and Future Work

The aim of this paper has been to present the WAF approach in the context of other schemes in the literature and illustrate its potential for generating new schemes, particularly in two and three dimensions. Our methods are, by definition, conservative and for appropriate integration schemes they are also second order accurate in space and time. In one dimension, we showed how well-known schemes such as the Lax Wendroff scheme [15], the Warming-Beam scheme [18] the MUSCL Hancock scheme [9], the PLM scheme of Colella [7] and the GRP method of Ben-Artzi and Falcovitz [8] can be described in terms of the WAF approach. In two space dimensions, we reproduced the first order scheme of Colella [16] and used the approach to derive two finite volume schemes that are second order accurate in space and time. As far as we know, these schemes are new. They have multidimensional upwinding aspects and good stability properties.

As an indication of their practical use, we showed how one of these schemes could be combined with the first order scheme on the linear advection equation using one dimensional TVD limiter functions to produce an (almost) oscillation-free scheme that is second order accurate in regions of smooth flow, and presented some numerical results. We then went on to derive the equivalent scheme in three dimensions.

Current work involves extending the two dimensional oscillation-free scheme of §3 to non-linear systems. The extension will be based on the on the wave model presented there. This work is already well underway, and we hope to communicate the results soon. Following directly from this will be the extension of the scheme to curvi-linear grids, and the development of the three dimensional scheme.

References

[1] S.K Godunov. A Finite Difference Method for the Computation of Discontinuous Solutions of the Equations of Fluid Dynamics. *Mat. Sb.*, 47:357–393, 1959.

[2] B van Leer. Towards the Ultimate Conservative Difference Scheme IV. A New Approach to Numerical Convection. *J. Comput. Phys*, 23:276–299, 1977.

[3] P.L. Roe. Approximate Riemann Solvers, Parameter Vectors, and Difference Schemes. *J. Comput. Phys*, 43:357–372, 1981.

[4] S. Osher and F. Solomon. Upwind Difference Schemes for Hyperbolic Conservation Laws. *Math. Comp.*, 38,158:339–374, 1982.

[5] A. Harten. On a Class of High Resolution Total Variation Stable Finite Difference Schemes. *SIAM J. Numer. Anal*, 21(1):1–23, 1984.

[6] B van Leer. Towards the Ultimate Conservative Difference Scheme III. Upstream-centered Finite Difference Schemes for Ideal Compressible Flow. *J. Comput. Phys*, 23:263–275, 1977.

[7] P. Colella. A Direct Eulerian MUSCL Scheme for Gas Dynamics. *SIAM J. Sci. Stat. Comput*, 6:104–117, 1985.

[8] M. Ben-Artzi and J. Falcovitz. A Second Order Godunov-Type Scheme for Compressible Fluid Dynamics. *J. Comput. Phys*, 55:1–32, 1985.

[9] J.J. Quirk. An Alternative to Unstructured Grids for Computing Gas Dynamic Flows Around Arbitrarily Complex Two Dimensional Bodies. Technical Report 92/7, ICASE, 1992.

[10] E.F. Toro. A Weighted Average Flux Method for Hyperbolic Conservation Laws. *Proc. Roy. Soc. Lond.*, A423:401–418, 1989.

[11] E.F. Toro. A New Numerical Technique for Quasi-Linear Hyperbolic Systems of Conservation Laws. Technical Report 8708, Cranfield CoA, 1987.

[12] E.F. Toro and P.L. Roe. A Hybridised High-Order Random Choice Method for Quasi-Linear Hyperbolic Systems. In Gronig, editor, *Proc. 16th Intern. Symp. on Shock Tubes and Waves*, pages 701–708, Aachen, Germany, July 1987.

[13] E.F. Toro. Riemann-Problem Based Techniques for Computing Reactive Two-Phase Flows. In Dervieux and Larrouturrou, editors, *Proc. Third. Intern. Confer. on Numerical Combustion*, number 351 in Lecture Notes in Physics, pages 472–481, Antibes, France, May 1989.

[14] E.F. Toro. The Weighted Average Flux Method Applied to the Time-Dependent Euler Equations. *Phil. Trans. Roy. Soc. Lond.*, A341:499–530, 1992.

[15] P. Lax and P. Wendroff. Systems of Conservation Laws. *Comm. Pure Appl. Math.*, pages 217–237, 1960.

[16] P. Colella. Multidimensional Upwind Methods for Hyperbolic Conservation Laws. *J. Comput. Phys*, 87:171–200, 1990.

[17] P.L. Roe. Numerical Algorithms for the Linear Wave Equation. Technical Report TR 81047, Royal Aircraft Establishment, 1981.

[18] R.F. Warming and R.W. Beam. Upwind Second Order Difference Schemes with Applications in Aerodynamic Flows. *AIAA Journal*, 24:1241–1249, 1976.

[19] V. Casulli and E.F Toro. Preliminary Results on a Semi-Lagrangian Version of the WAF Method. Technical Report 9018, College of Aeronautics, Cranfield Institute of Technology, U.K., 1990.

[20] E.F. Toro and S.J. Billett. A Unified, Riemann Problem Based Extension of the Warming-Beam and Lax-Wendroff Methods. In H. Daiguji, editor, *Proceedings of the Fifth International Symposium on Computational Fluid Dynamics*, volume III, pages 243–248, Tohoku University, Sendai, Japan, September 1993.

[21] E.F. Toro and S.J. Billett. A WAF Type Extension of the Warming-Beam and Lax-Wendroff Schemes. (in preparation).

[22] W. Speares. A Finite Volume Approach to the Weighted Average Flux Method. MSc thesis, Cranfield Institute of Technology, U.K., 1991.

[23] C. Hirsch. Numerical Computation of Internal and External Flows. Wiley, 1988.

[24] R. LeVeque. High Resolution Finite Volume Methods on Arbitrary Grids via Wave Propagation. *J. Comput. Phys*, 78:36–63, 1988.

[25] A. Harten. High Resolution Schemes for Hyperbolic Conservation Laws. *J. Comput. Phys*, 49:357–393, 1983.

[26] P.K. Sweby. High Resolution Schemes Using Flux Limiters for Hyperbolic Conservation Laws. *SIAM J. Numer. Anal.*, 21:995–1011, 1984.

[27] J.B. Goodman and R.J LeVeque. On the Accuracy of Stable Schemes for 2D Scalar Conservation Laws. *Math. Comp.*, 45(21):15–21, 1985.

[28] P. Tamamidis and D.N. Assanis. Evaluation of Various High-Order-Accuracy Schemes With and Without Flux Limiters. *Int. J. Num. Meth. Fluids*, 16:931–948, 1993.

Legends to figures

Figure 1 The integration range and wave structure for $\Delta T_\nu(0, \frac{1}{2})$.

Figure 2 The integration range and wave structure for $\Delta T_\nu(\frac{1}{2}, 1)$.

Figure 3 The general integration range.

Figure 4a Space integration range for the fluxes $\mathbf{f}_{i+\frac{1}{2},j}$.

Figure 4b Space integration range for the fluxes $\mathbf{g}_{i,j+\frac{1}{2}}$.

Figure 5 The integral for the intercell flux $\mathbf{f}_{i+\frac{1}{2},j}$ in two dimensions: exact integration in all directions. The flow is moving *into* the page.

Figure 6 The stencil for the second order schemes: full circles denote upwind points, empty circles denote downwind points.

Figure 7a Two dimensional integration range: Exact integration in time, exact integration perpendicular to the boundary, and the midpoint rule parallel to the boundary.

Figure 7b Two dimensional integration range: Exact integration in time, exact integration parallel to the boundary, and the midpoint rule perpendicular to the boundary.

Figure 7c Two dimensional integration range: Exact integration in time, and the midpoint rule in both space directions.

Figure 8 Integration using midpoint rule in time and exact integration is both space directions: status of the space integration range at time $t = \frac{1}{2}\Delta t$.

Figure 9 Stability diagrams for the two dimensional schemes.

Figure 10 Labeling of the boundaries for the two dimensional wave model.
Constant wavespeed case.
Boundary 4 is the boundary across which the flux in being calculated.

Figure 11 Weights for the two-dimensional wave model.

Figure 12 Labeling of the boundaries for the two dimensional wave model.
Variable wavespeed case.
Boundary 4 is the boundary across which the flux in being calculated.

Figure 13a Advection of a square in two dimensions using the first order scheme.

Figure 13b Advection of a square in two dimensions using the VAN LEER limiter.

Figure 14a Exact solution to the warm/cold front problem at times 1.0, 2.0, 3.0 and 4.0 units.

Figure 14b Numerical solution to the warm/cold front problem at times 1.0, 2.0, 3.0 and 4.0 units using the VAN LEER limiter.

Figure 15 The three dimensional space integration range for $\mathbf{f}_{i+\frac{1}{2},j,k}$.

Figure 16 Integration for the 3D scheme: midpoint rule in time, exact integration in all space directions. The status of the space integration range at time $t = \frac{1}{2}\Delta t$.

Figure 17 Stability diagrams for the three dimensional second order scheme.

Figure 18 Integration range for $\mathbf{f}_{i+\frac{1}{2},j,k}$ for the first order scheme in three dimensions: Midpoint rule in time, midpoint rule perpendicular to the boundary and exact integration in both directions parallel to the boundary.

Figure 19 Labeling of the twelve boundaries contributing to the three dimensions second order flux. Boundary 1 is the boundary across which the flux is being calculated. The flow is moving *into* the page, and *upwards*. Circles indicate the boundary 'behind'.

Figure 20 Integration for the weights in the 3D wave model — the volume for boundary 1. The flow is moving *into* the page, and *upwards*.

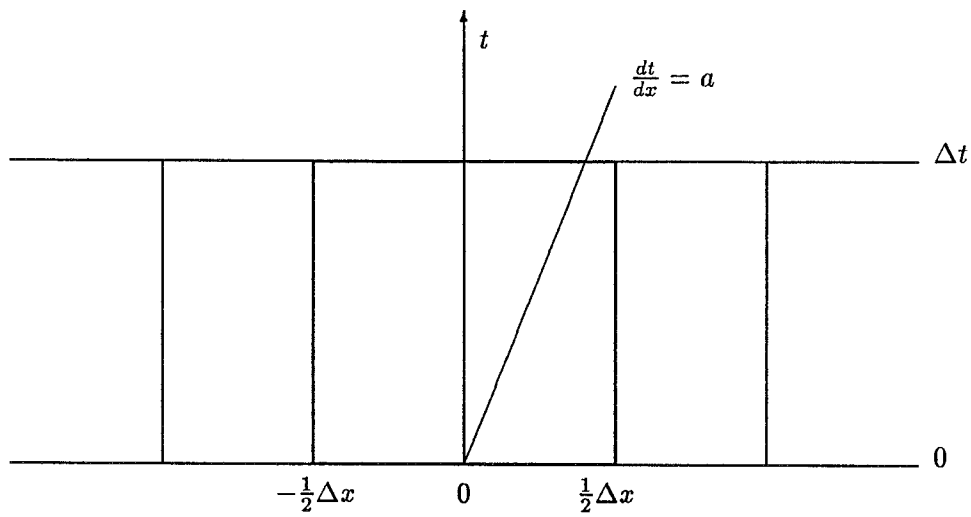

Figure 1 The integration range and wave structure for $\Delta T_\nu(0, \frac{1}{2})$.

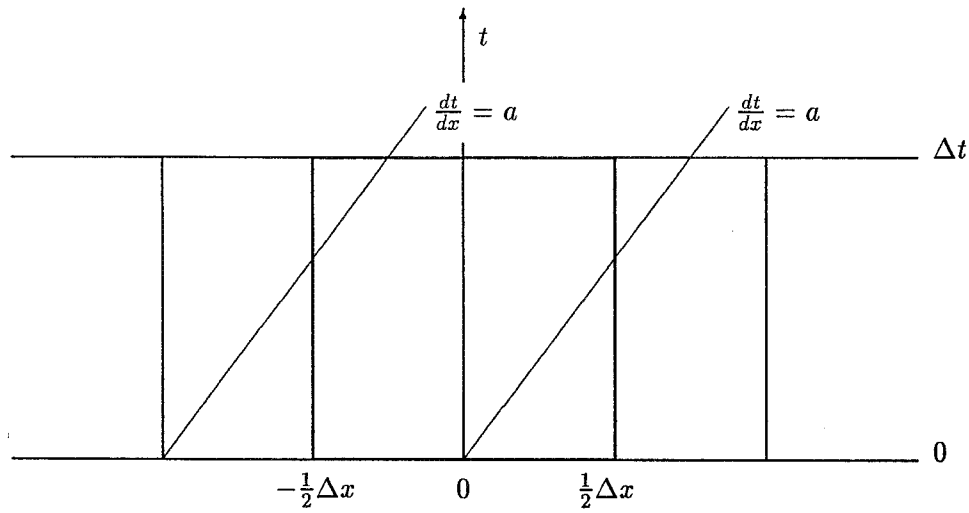

Figure 2 The integration range and wave structure for $\Delta T_\nu(\frac{1}{2}, 1)$.

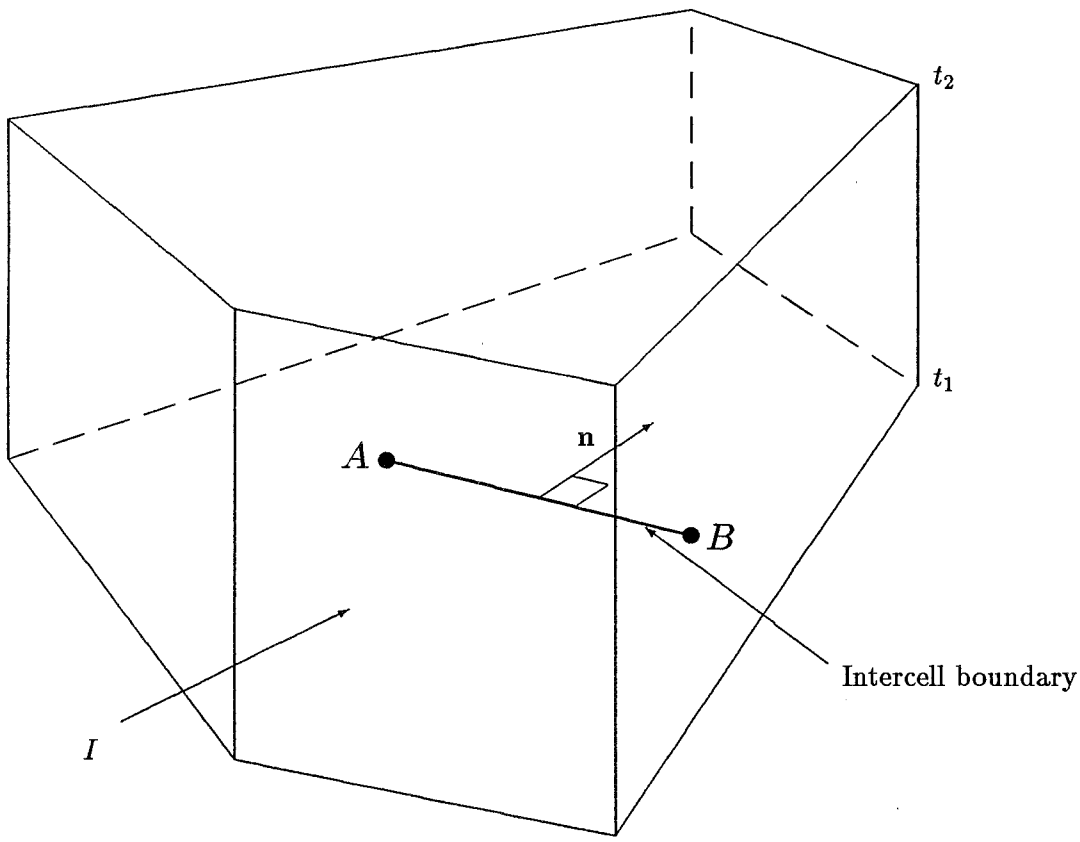

Figure 3 The general integration range.

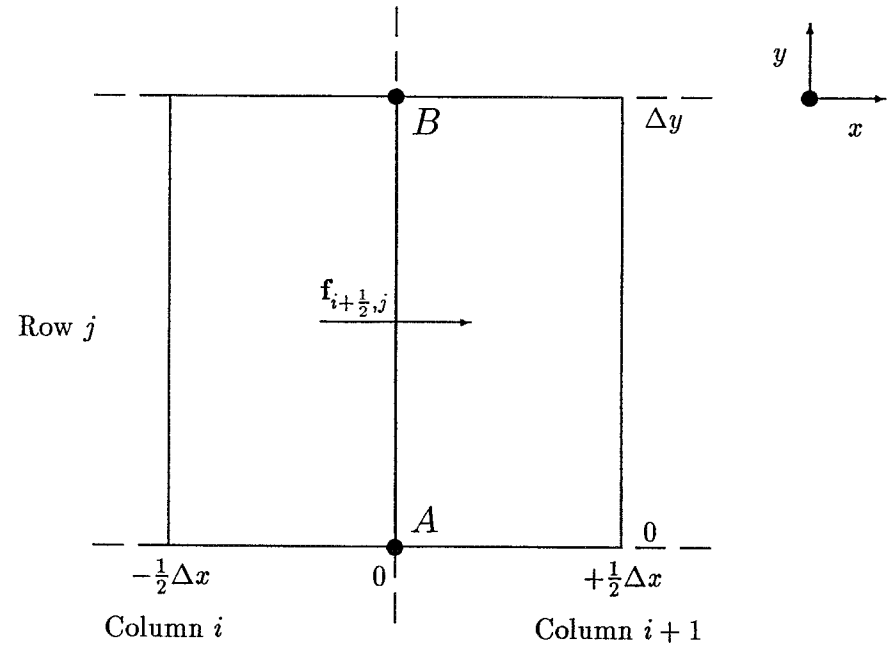

Figure 4a Space integration range for the fluxes $\mathbf{f}_{i+\frac{1}{2},j}$.

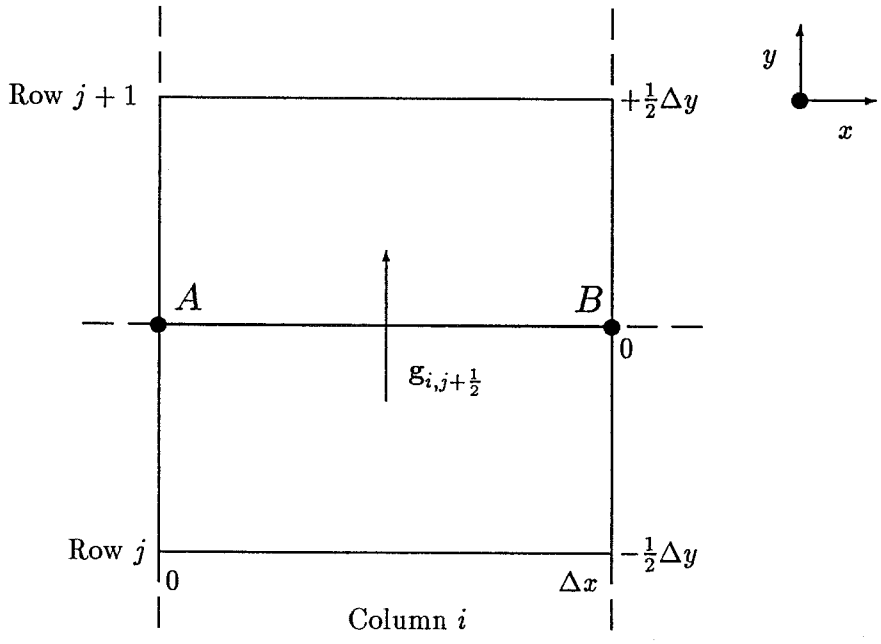

Figure 4b Space integration range for the fluxes $\mathbf{g}_{i,j+\frac{1}{2}}$.

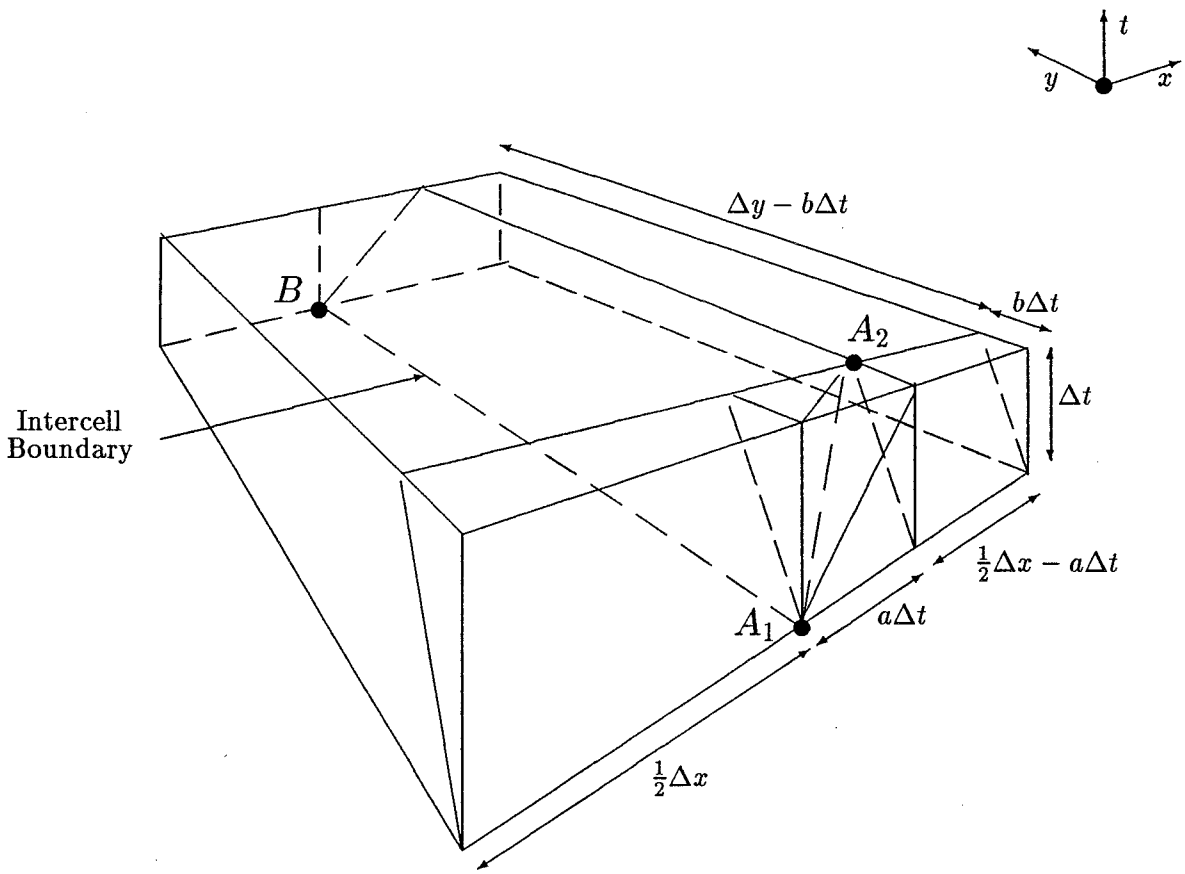

Figure 5 The integral for the intercell flux $\mathbf{f}_{i+\frac{1}{2},j}$ in two dimensions: exact integration in all directions. The flow is moving *into* the page.

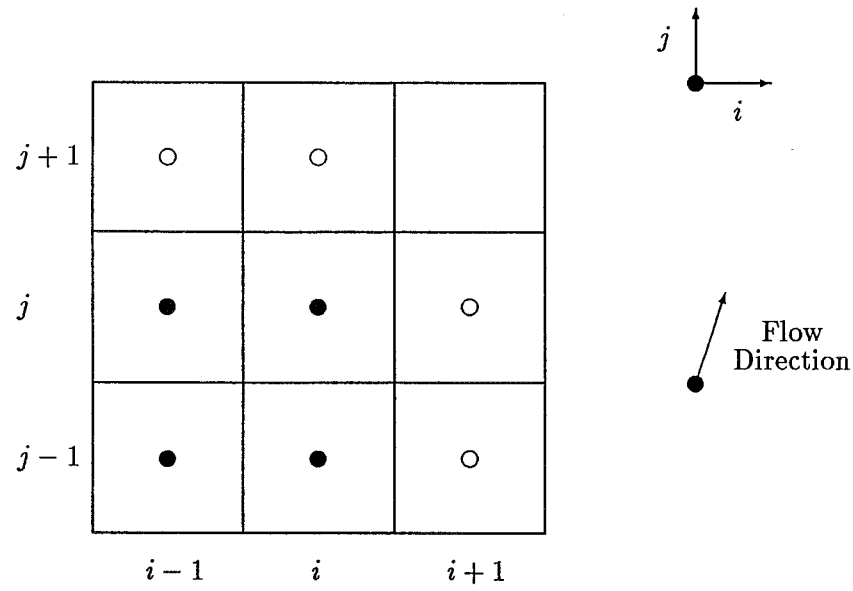

Figure 6 The stencil for the second order schemes: full circles denote upwind points, empty circles denote downwind points.

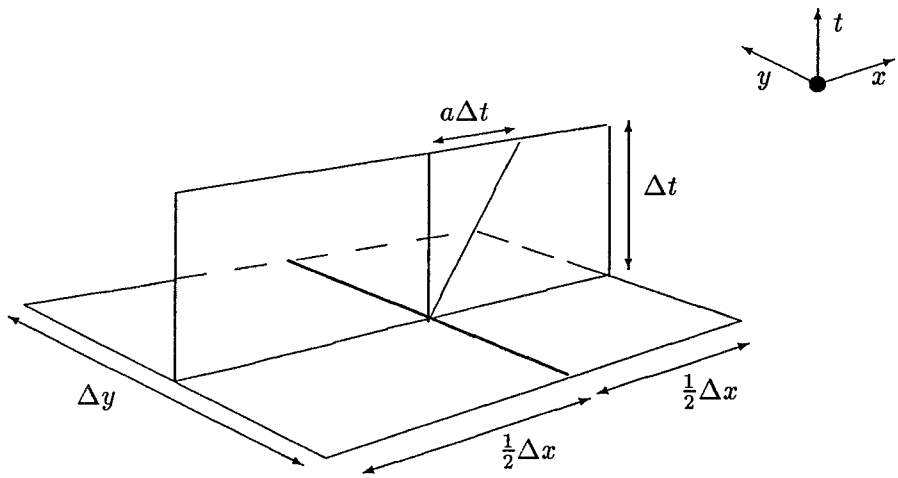

Figure 7a Two dimensional integration range: Exact integration in time, exact integration perpendicular to the boundary, and the midpoint rule parallel to the boundary.

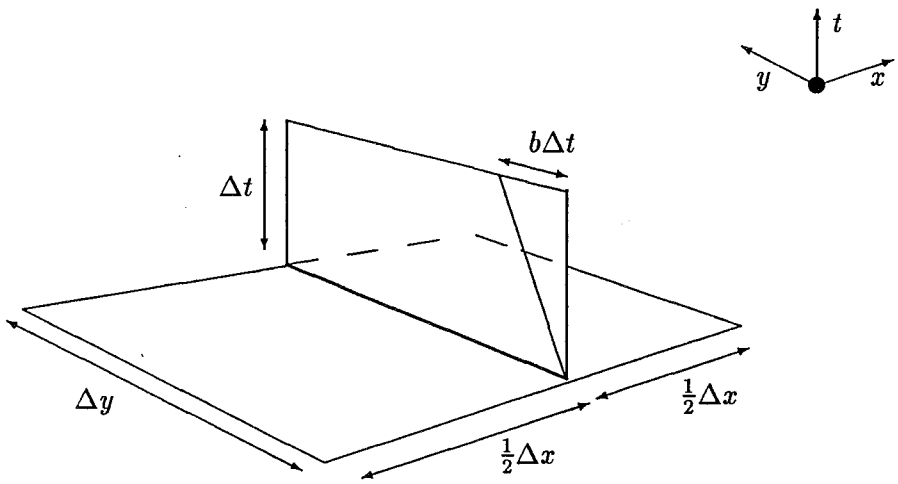

Figure 7b Two dimensional integration range: Exact integration in time, exact integration parallel to the boundary, and the midpoint rule perpendicular to the boundary.

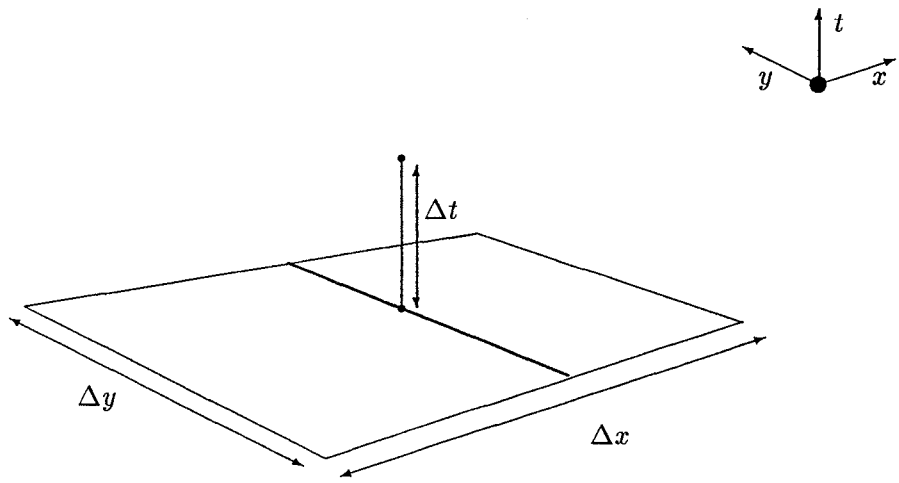

Figure 7c Two dimensional integration range: Exact integration in time, and the midpoint rule in both space directions.

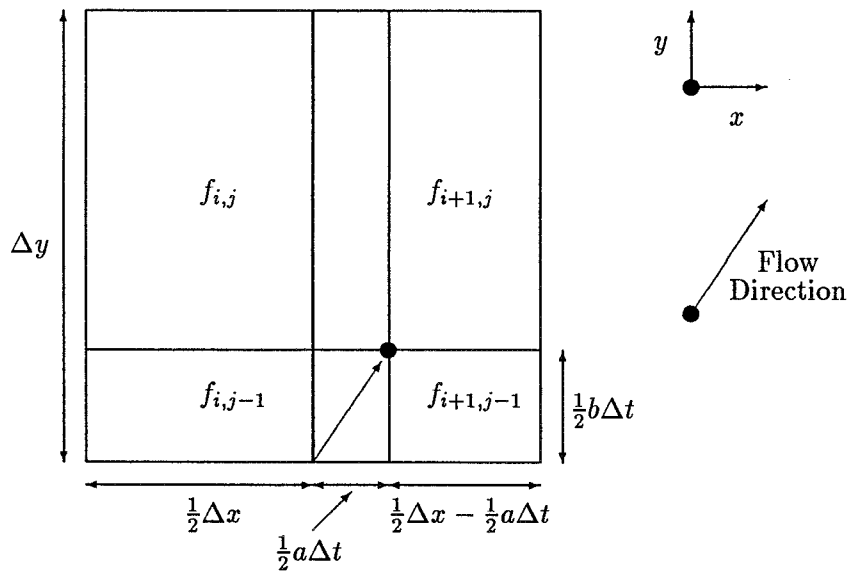

Figure 8 Integration using midpoint rule in time and exact integration is both space directions: status of the space integration range at time $t = \frac{1}{2}\Delta t$.

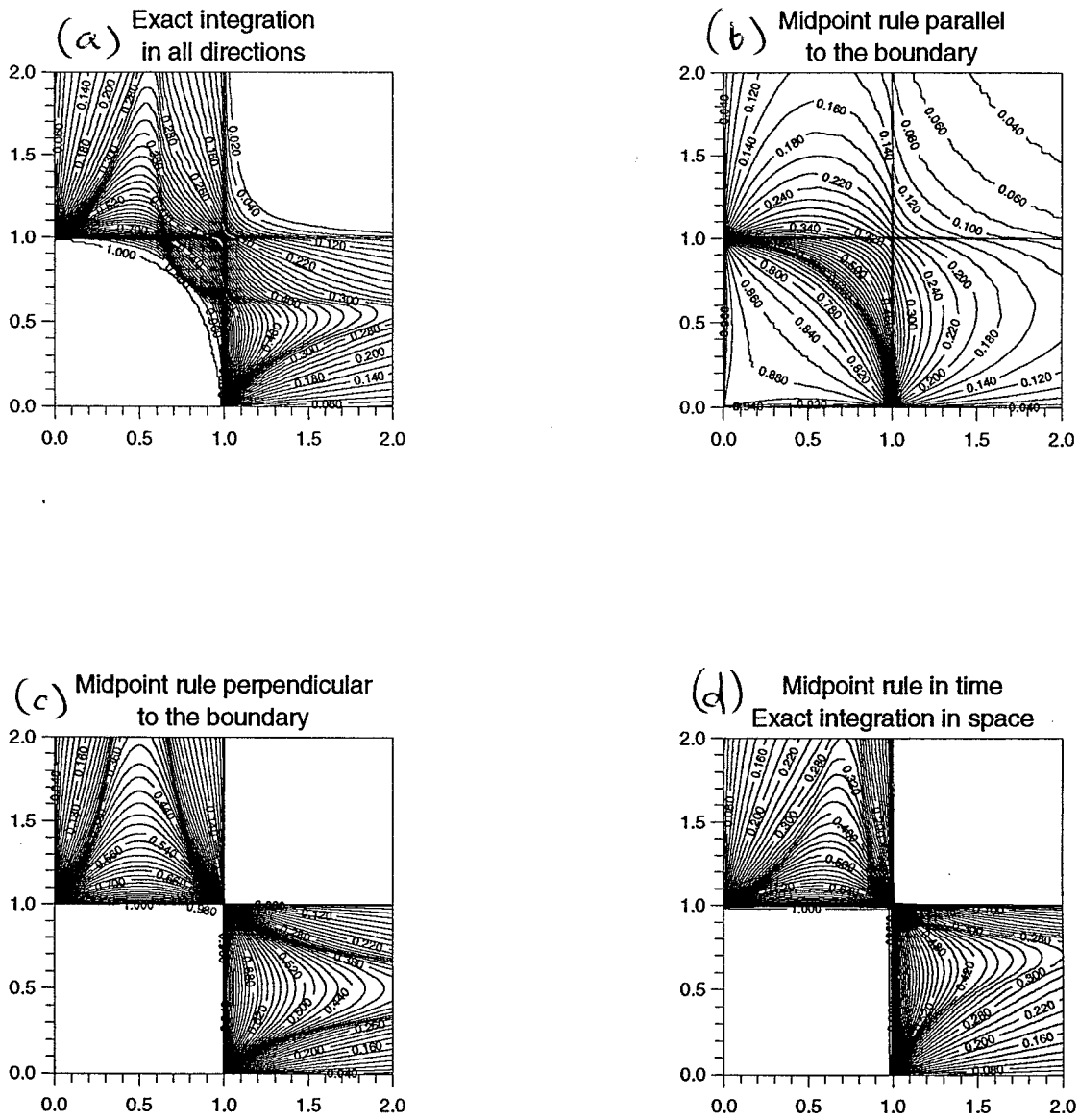

Figure 9 Stability diagrams for the two dimensional schemes.

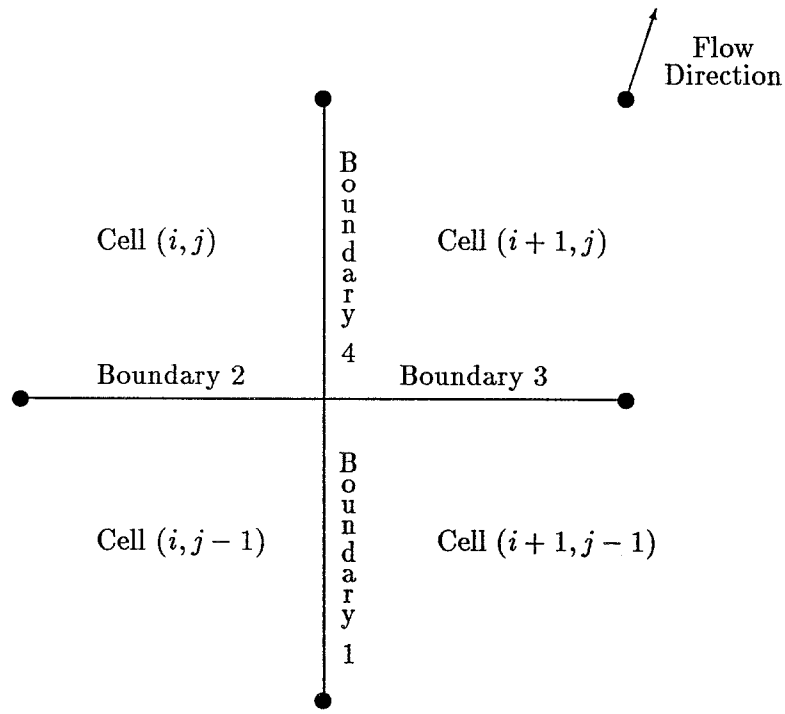

Figure 10 Labeling of the boundaries for the two dimensional wave model.
Constant wavespeed case.
Boundary 4 is the boundary across which the flux in being calculated.

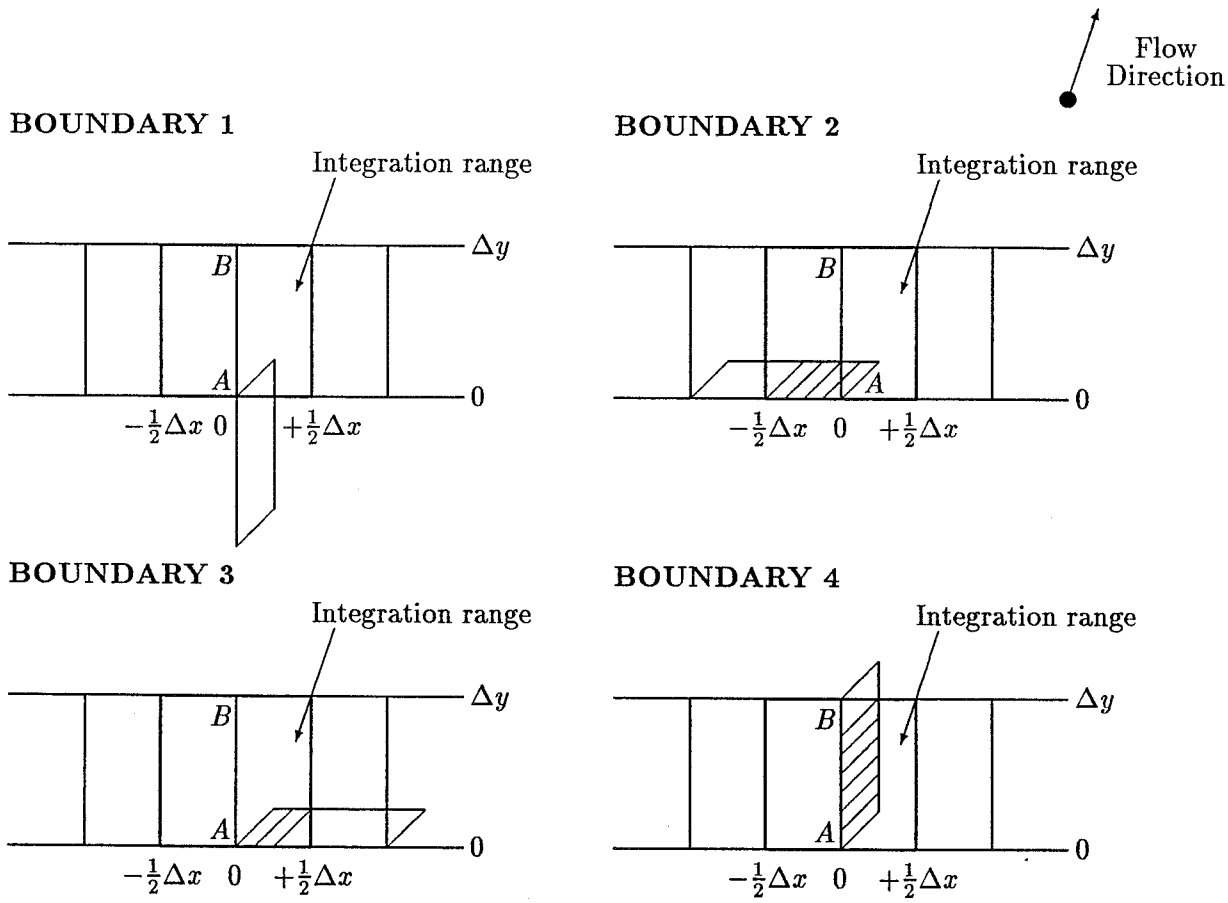

Figure 11 Weights for the two-dimensional wave model.

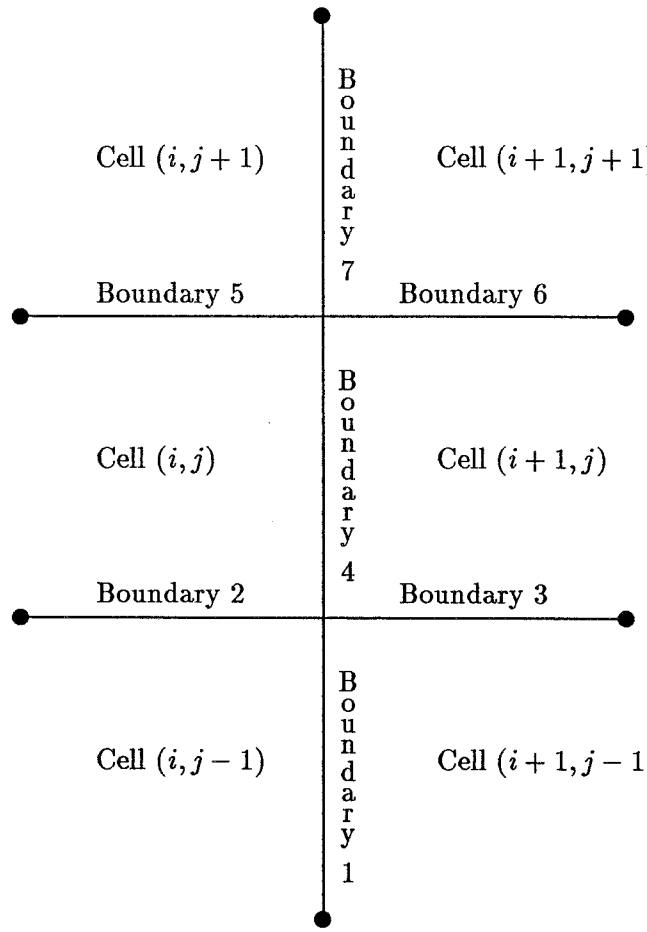

Figure 12 Labeling of the boundaries for the two dimensional wave model.
Variable wavespeed case.
Boundary 4 is the boundary across which the flux in being calculated.

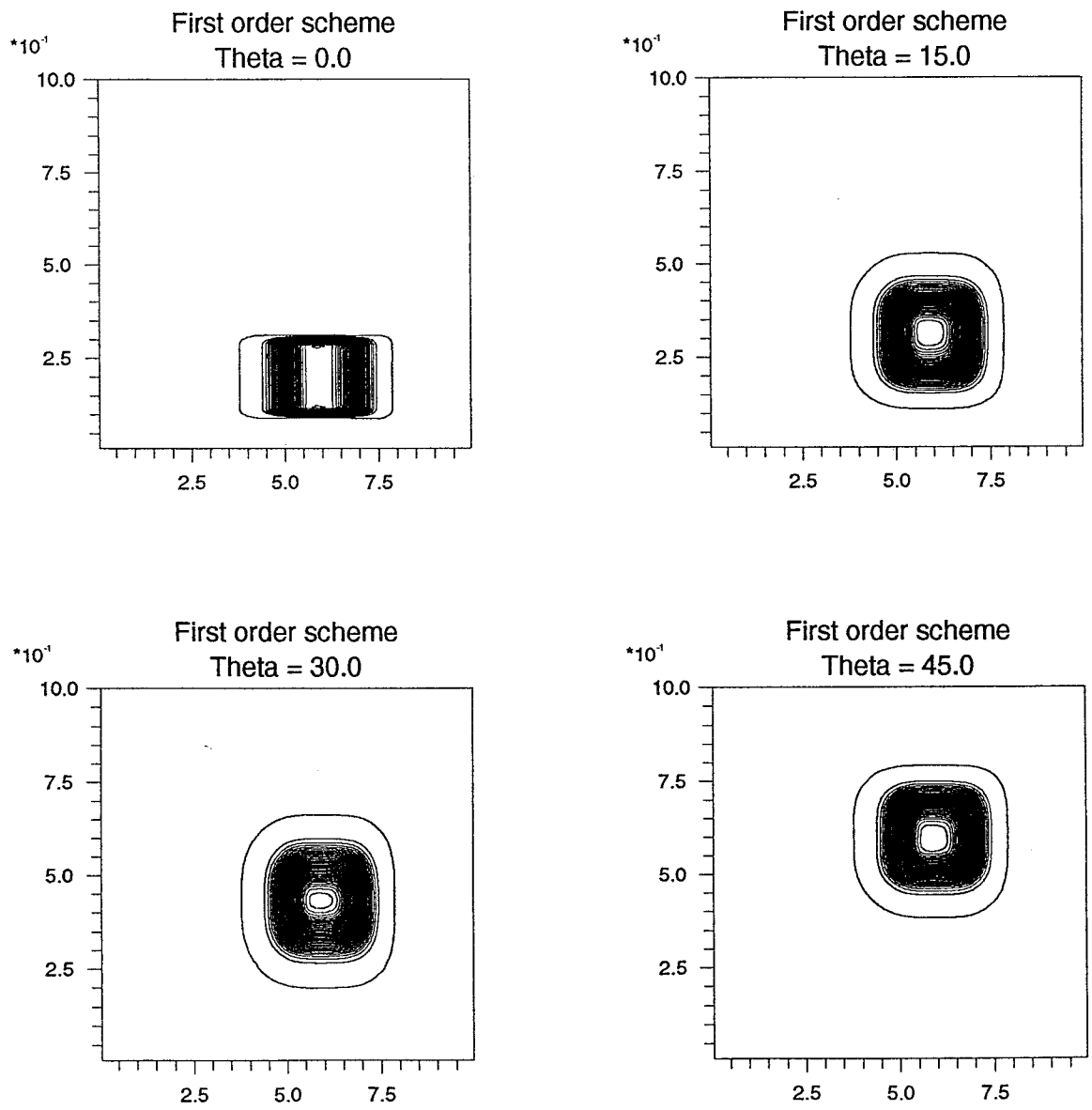

Figure 13a Advection of a square in two dimensions using the first order scheme.

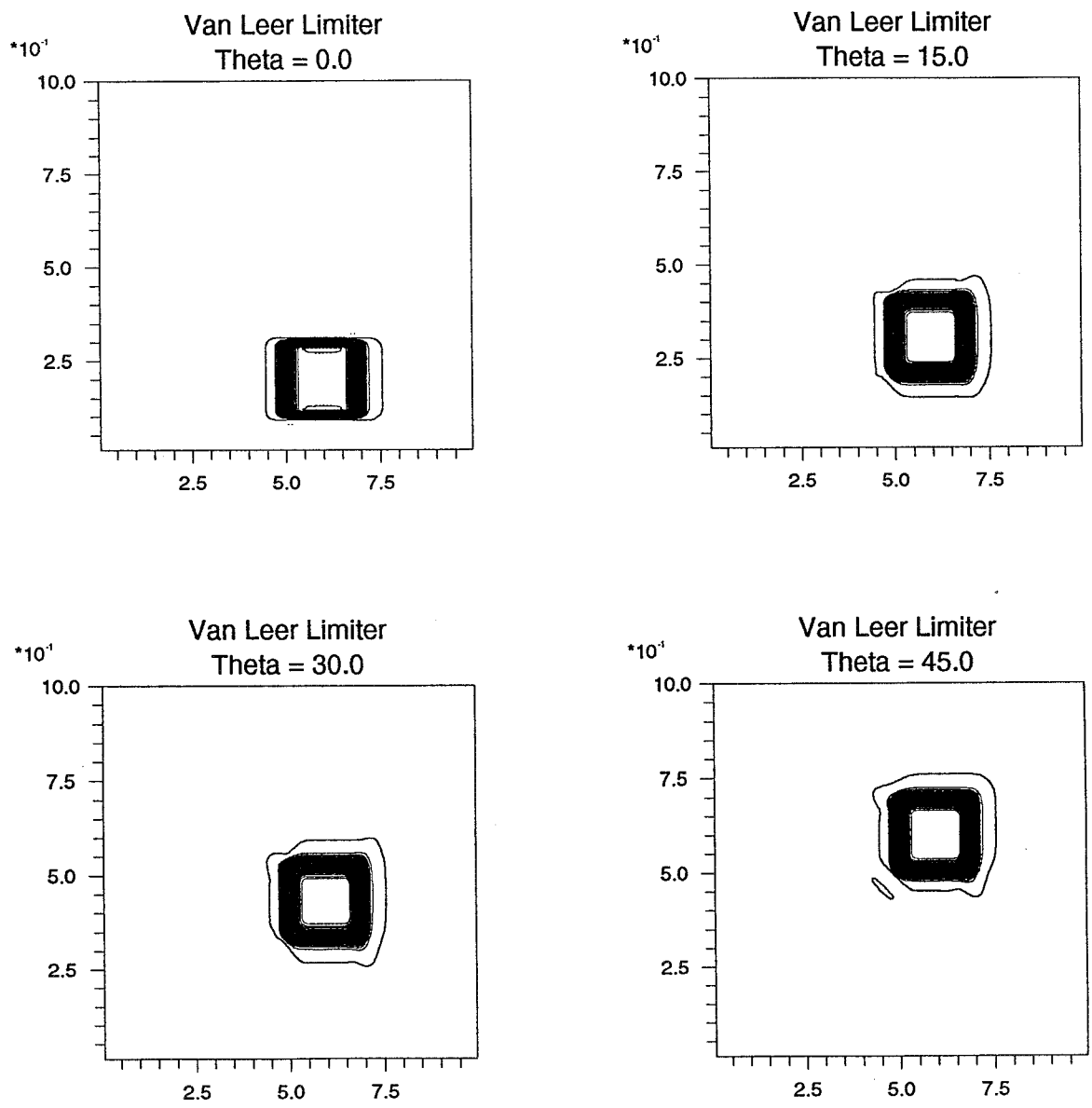

Figure 13b Advection of a square in two dimensions using the VAN LEER limiter.

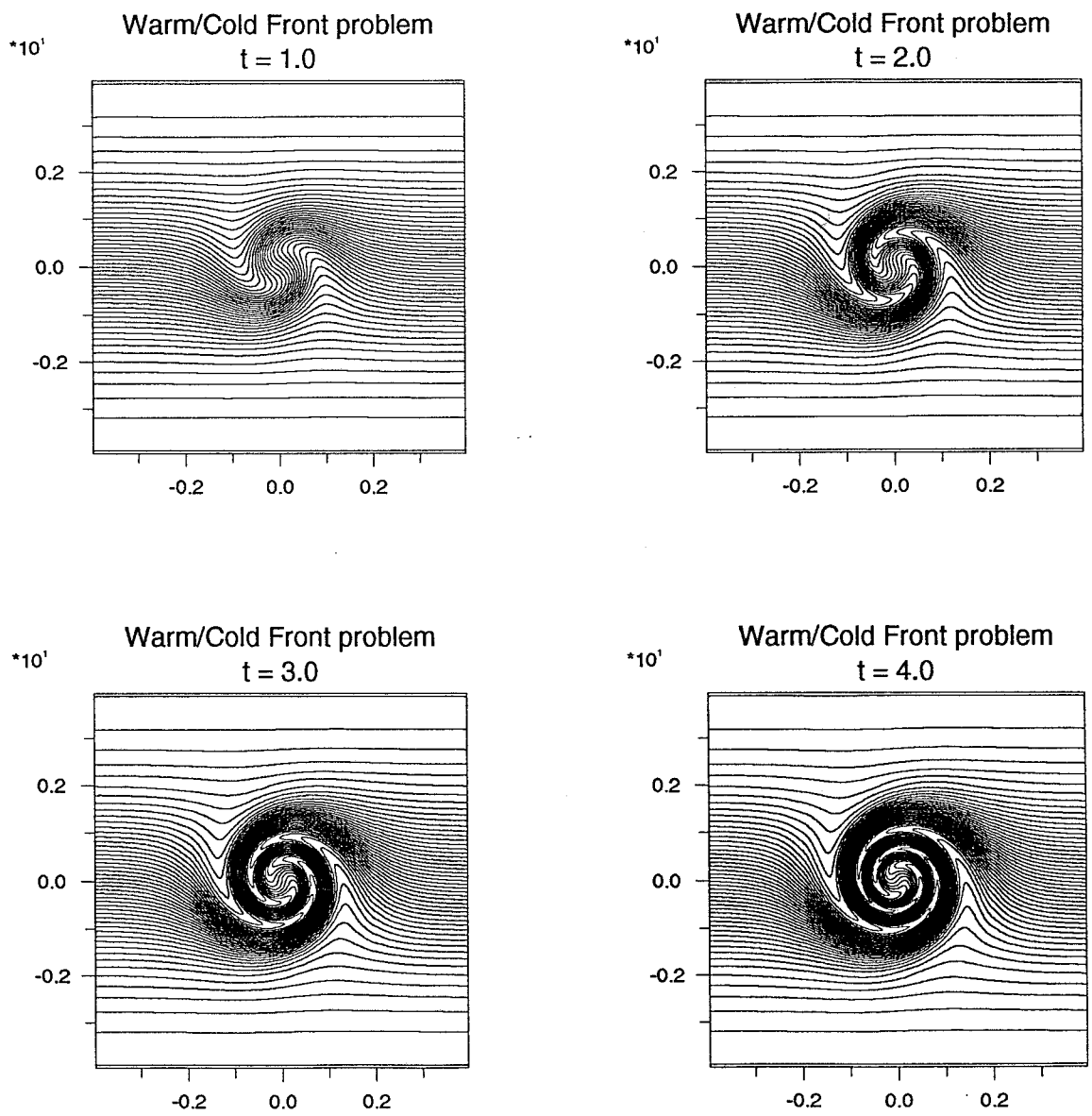

Figure 14a Exact solution to the warm/cold front problem at times 1.0, 2.0, 3.0 and 4.0 units.

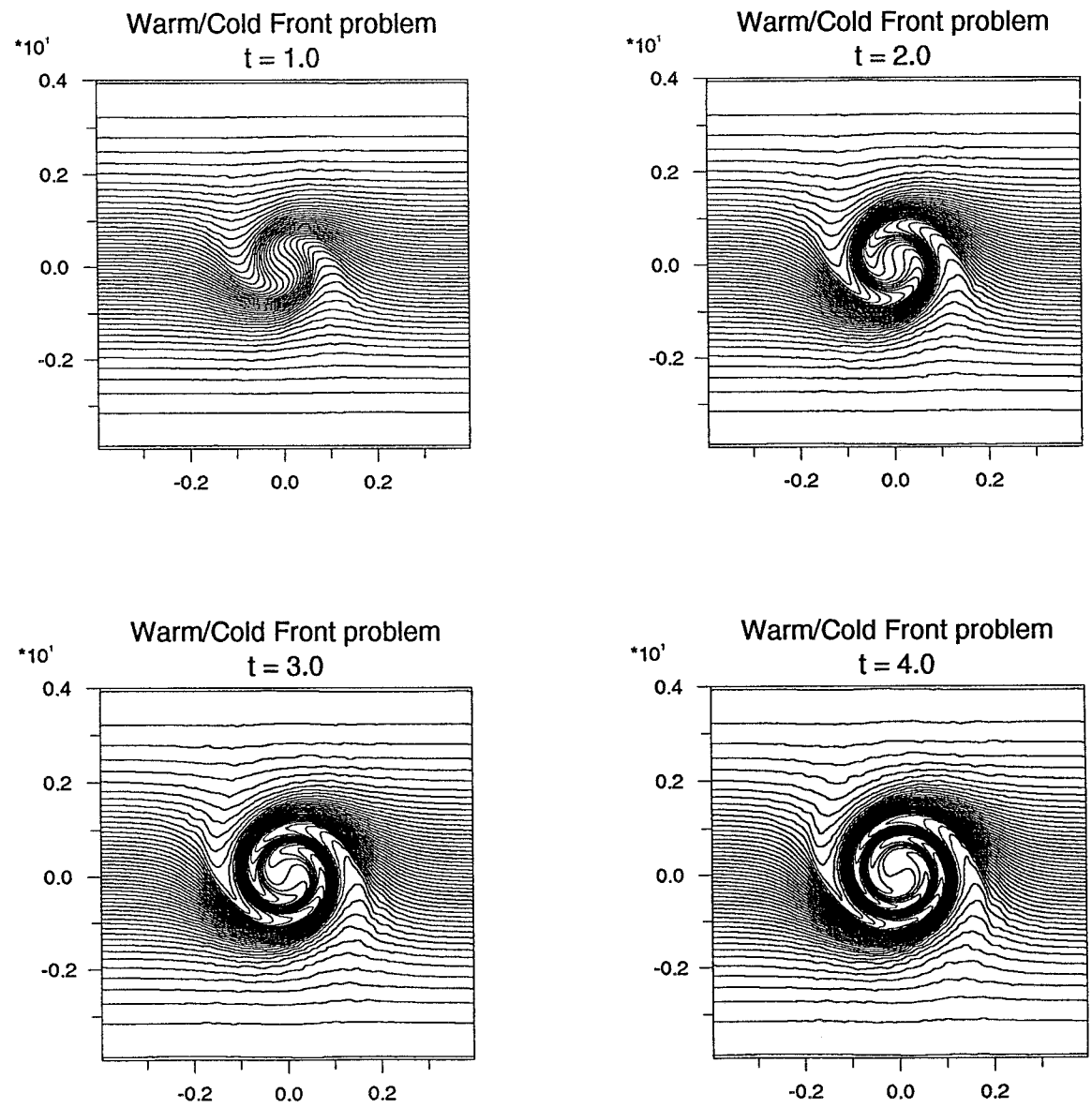

Figure 14b Numerical solution to the warm/cold front problem at times 1.0, 2.0, 3.0 and 4.0 units using the VAN LEER limiter.

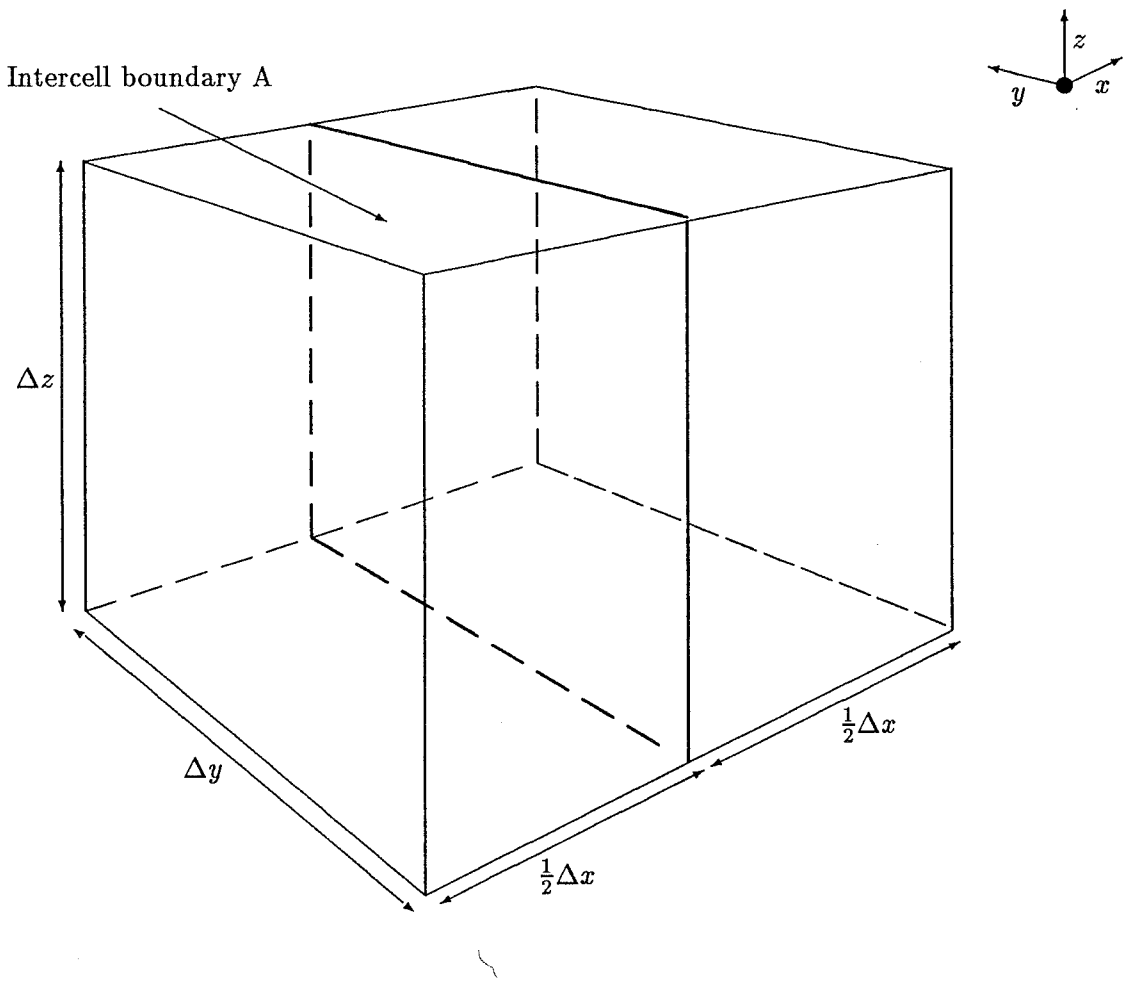

Figure 15 The three dimensional space integration range for $\mathbf{f}_{i+\frac{1}{2},j,k}$.

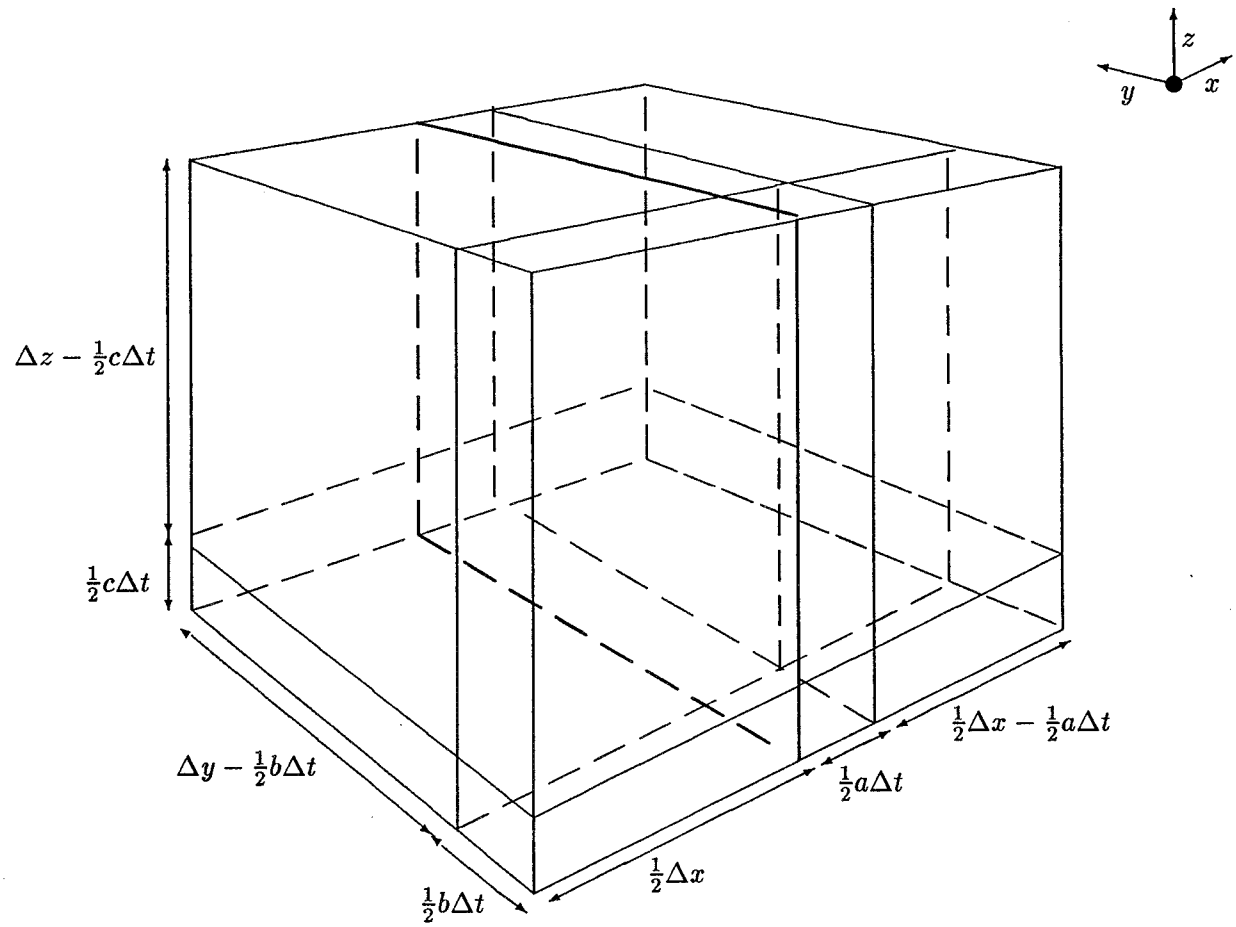

Figure 16 Integration for the 3D scheme: midpoint rule in time, exact integration in all space directions. The status of the space integration range at time $t = \frac{1}{2}\Delta t$.

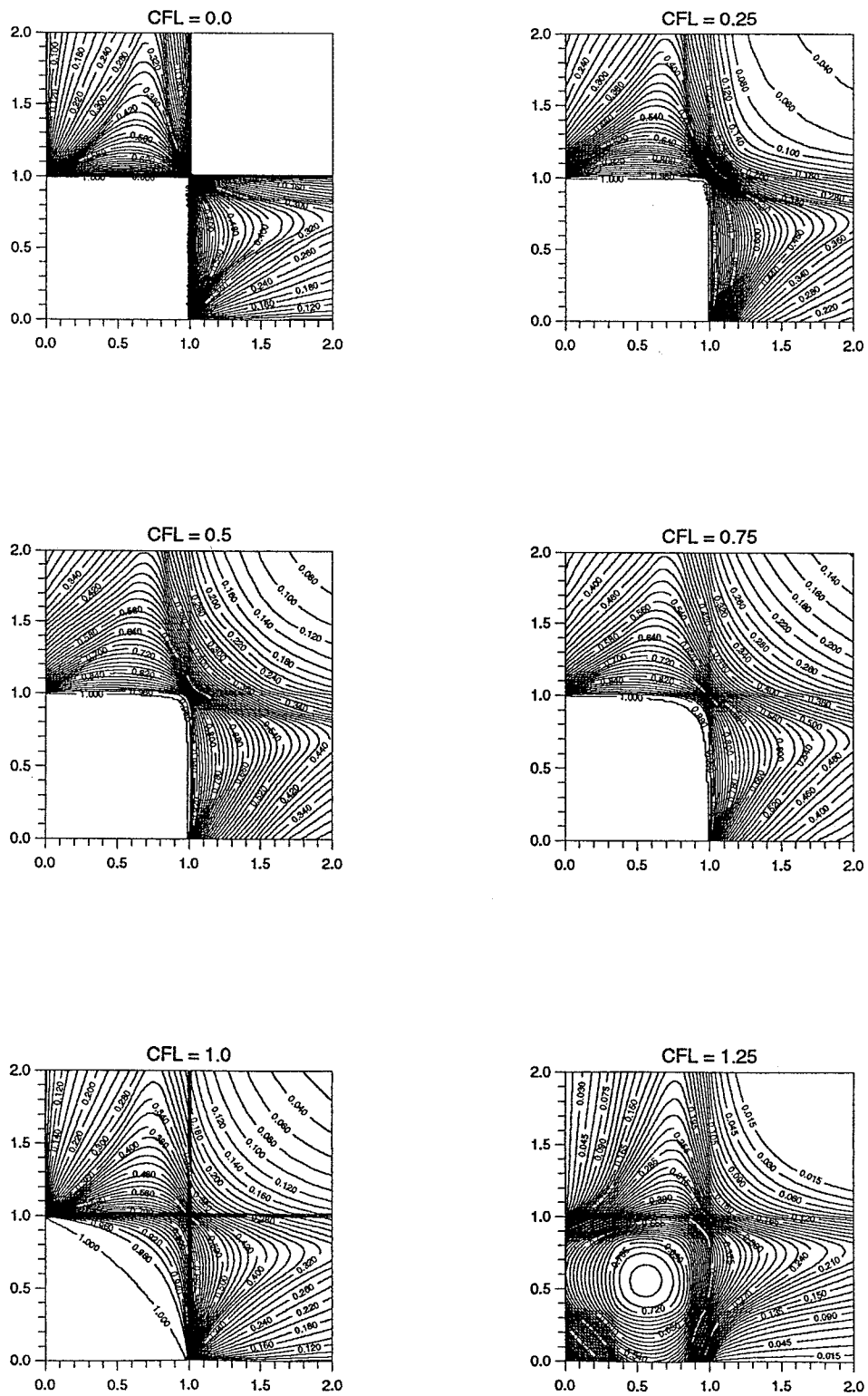

Figure 17 Stability diagrams for the three dimensional second order scheme.

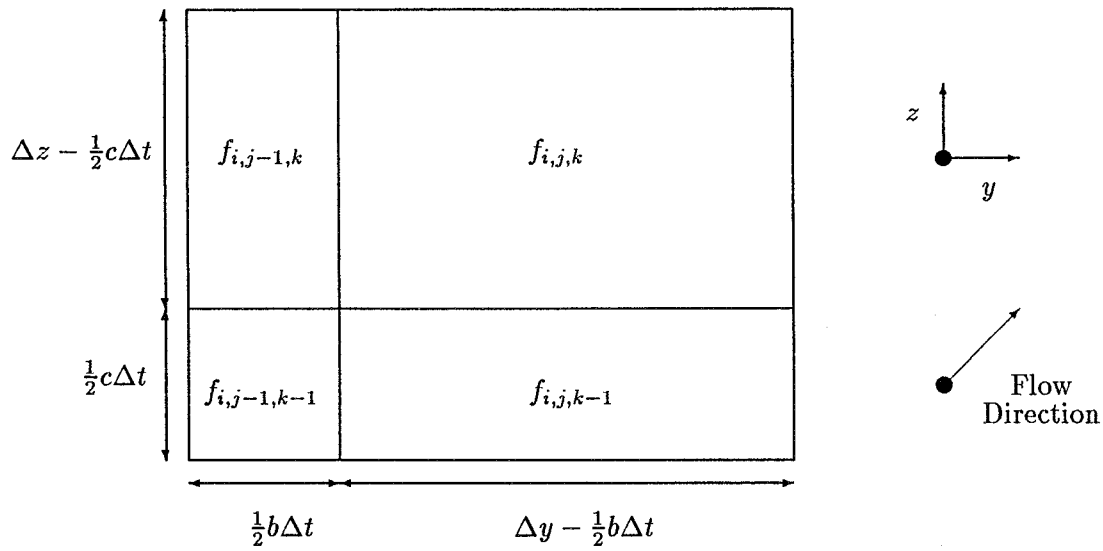

Figure 18 Integration range for $\mathbf{f}_{i+\frac{1}{2},j,k}$ for the first order scheme in three dimensions: Midpoint rule in time, midpoint rule perpendicular to the boundary and exact integration in both directions parallel to the boundary.

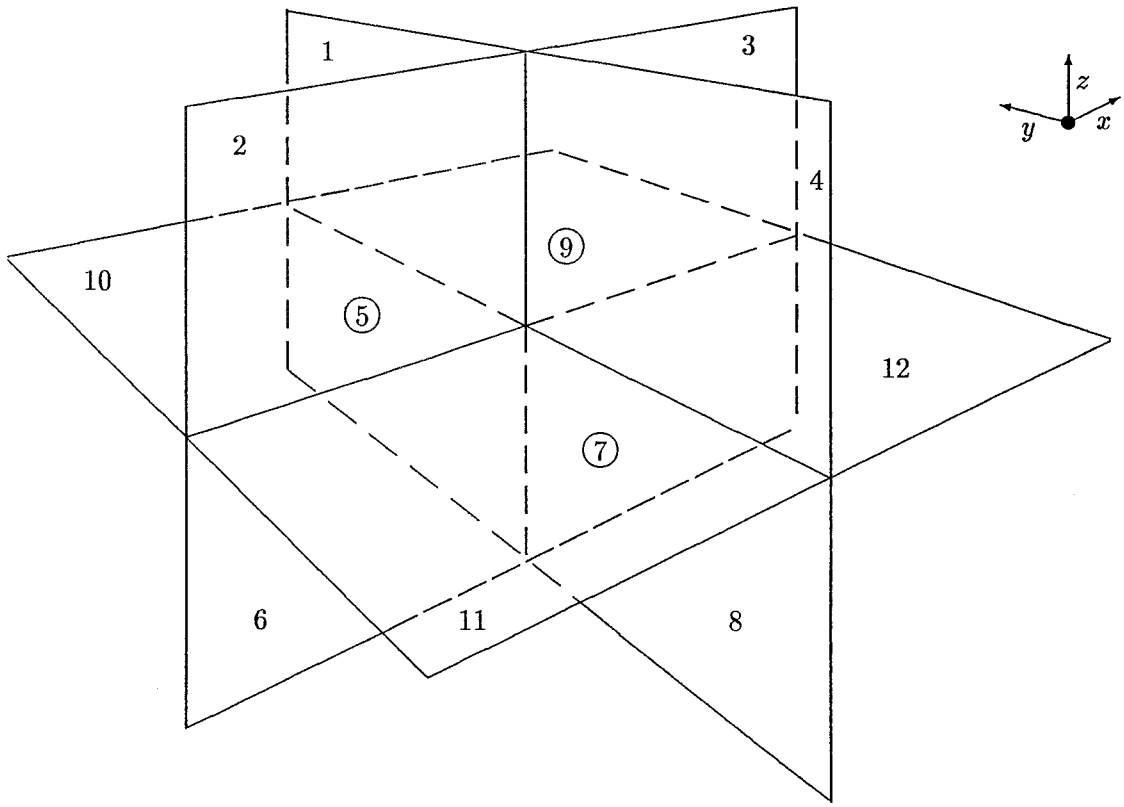

Figure 19 Labeling of the twelve boundaries contributing to the three dimensions second order flux.
Boundary 1 is the boundary across which the flux is being calculated.
The flow is moving *into* the page, and *upwards.*
Circles indicate the boundary 'behind'.

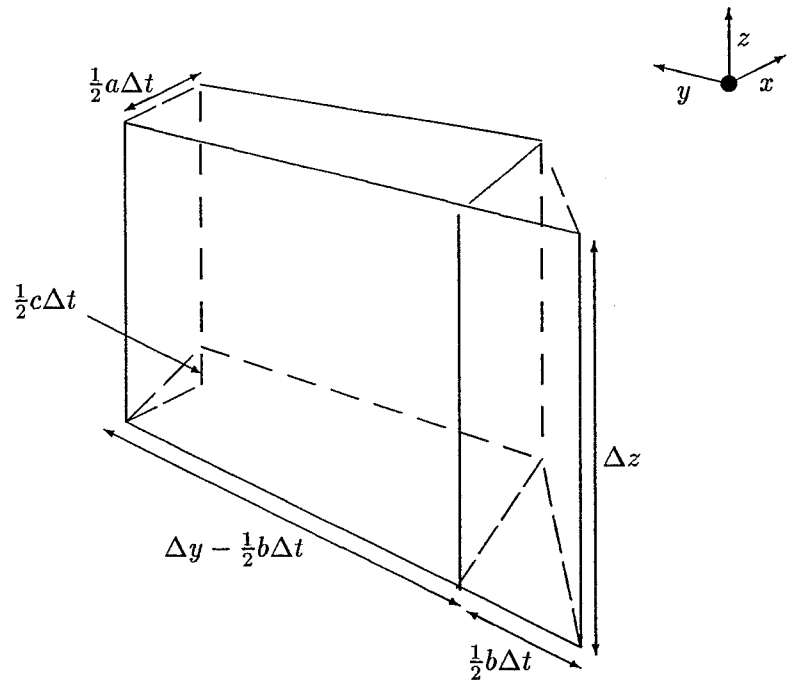

Figure 20 Integration for the weights in the 3D wave model — the volume for boundary 1. The flow is moving *into* the page, and *upwards*.